The Journal of Immunology

Differential Activation of Hepatic Invariant NKT Cell Subsets Plays a Key Role in Progression of Nonalcoholic Steatohepatitis

Igor Maricic, Idania Marrero, Akiko Eguchi, Ryota Nakamura, Casey D. Johnson, Suryasarathi Dasgupta, Carolyn D. Hernandez, Phirum Sam Nguyen, Austin D. Swafford, Rob Knight, Ariel E. Feldstein, Rohit Loomba and Vipin Kumar

J Immunol 2018; 201:3017-3035; Prepublished online 15 October 2018;
doi: 10.4049/jimmunol.1800614
http://www.jimmunol.org/content/201/10/3017

The Journal of Immunology is published twice each month by
The American Association of Immunologists, Inc.,
1451 Rockville Pike, Suite 650, Rockville, MD 20852

Print ISSN: 0022-1767 Online ISSN: 1550-6606.

Differential Activation of Hepatic Invariant NKT Cell Subsets Plays a Key Role in Progression of Nonalcoholic Steatohepatitis

Igor Maricic,*[,1] Idania Marrero,*[,1] Akiko Eguchi,[†] Ryota Nakamura,[†] Casey D. Johnson,[†] Suryasarathi Dasgupta,* Carolyn D. Hernandez,* Phirum Sam Nguyen,* Austin D. Swafford,[‡] Rob Knight,[†,‡,§] Ariel E. Feldstein,[†,¶] Rohit Loomba,*[,‡,¶] and Vipin Kumar*[,‡,¶]

Innate immune mechanisms play an important role in inflammatory chronic liver diseases. In this study, we investigated the role of type I or invariant NKT (iNKT) cell subsets in the progression of nonalcoholic steatohepatitis (NASH). We used α-galactosylceramide/CD1d tetramers and clonotypic mAb together with intracytoplasmic cytokine staining to analyze iNKT cells in choline-deficient L-amino acid–defined (CDAA)-induced murine NASH model and in human PBMCs, respectively. Cytokine secretion of hepatic iNKT cells in CDAA-fed C57BL/6 mice altered from predominantly IL-17$^+$ to IFN-γ$^+$ and IL-4$^+$ during NASH progression along with the downmodulation of TCR and NK1.1 expression. Importantly, steatosis, steatohepatitis, and fibrosis were dependent upon the presence of iNKT cells. Hepatic stellate cell activation and infiltration of neutrophils, Kupffer cells, and CD8$^+$ T cells as well as expression of key proinflammatory and fibrogenic genes were significantly blunted in Jα18$^{-/-}$ mice and in C57BL/6 mice treated with an iNKT-inhibitory RAR-γ agonist. Gut microbial diversity was significantly impacted in Jα18$^{-/-}$ and in CDAA diet–fed mice. An increased frequency of CXCR3$^+$IFN-γ$^+$T-bet$^+$ and IL-17A$^+$ iNKT cells was found in PBMC from NASH patients in comparison with nonalcoholic fatty liver patients or healthy controls. Consistent with their in vivo activation, iNKT cells from NASH patients remained hyporesponsive to ex-vivo stimulation with α-galactosylceramide. Accumulation of plasmacytoid dendritic cells in both mice and NASH patients suggest their role in activation of iNKT cells. In summary, our findings indicate that the differential activation of iNKT cells play a key role in mediating diet-induced hepatic steatosis and fibrosis in mice and its potential involvement in NASH progression in humans. ***The Journal of Immunology*****, 2018, 201: 3017–3035.**

Nonalcoholic fatty liver disease (NAFLD) is the most frequent chronic liver disease that affects 10–20% of the population in developed countries and is increasing in prevalence with the rise of diabetes and obesity (1–3). NAFLD is characterized by abnormal accumulation of fat within liver or steatosis (nonalcoholic fatty liver [NAFL]) that can progress to severe inflammatory cell infiltration or nonalcoholic steatohepatitis (NASH) accompanied by necrosis and fibrosis that can lead to liver cirrhosis and hepatocellular carcinoma (4). A detailed understanding of the cellular and molecular mechanisms involved in progression from steatosis to fibrosis in NAFLD is lacking, and they are crucial in the development of effective therapeutic approaches to halt this disease.

Different unconventional innate-like T cells, including γδ-T cells, mucosal-associated invariant T (MAIT) cells, and NKT cells, are enriched in liver, where they can play a key role in immune homeostasis. NKT cells are the major innate-like T cells in the liver of both mice and humans. NKT cells recognize both self and microbial lipids presented by the MHC class I–like molecule CD1d (5). CD1d-restricted NKT cells have been shown to play an important role in inflammatory conditions, including autoimmune and infectious diseases (6–9).

NKT cells can be divided in two main subsets, type I or invariant NKT (iNKT) and type II, based upon differences in TCR characteristics and some of the Ags they recognize. Although both

*Division of Gastroenterology, Department of Medicine, University of California San Diego, La Jolla, CA 92093; [†]Department of Pediatrics, University of California San Diego, La Jolla, CA 92093; [‡]Center for Microbiome Innovation, University of California San Diego, La Jolla, CA 92093; [§]Department of Computer Science and Engineering, University of California San Diego, La Jolla, CA 92093; and [¶]Nonalcoholic Fatty Liver Disease Research Center, University of California San Diego, La Jolla, CA 92093

[1]I. Maricic and I. Marrero contributed equally to this work.

ORCIDs: 0000-0002-5793-706X (I. Marrero); 0000-0001-5655-8300 (A.D.S.); 0000-0002-4845-9991 (R.L.).

Received for publication May 1, 2018. Accepted for publication September 7, 2018.

This work was supported by National Institutes of Health Grants AA020864 (National Institutes for Alcohol Abuse and Alcoholism) and CA100660 (National Cancer Institute) to V.K. The University of California San Diego Neuroscience Core for Microscopy was supported by National Institutes of Health Grant NS047101 from the National Institute of Neurological Disorders and Stroke. The investigation of the mouse microbiome was supported by a Seed Grant from the University of California San Diego Center for Microbiome Innovation.

Address correspondence and reprint request to Prof. Vipin Kumar, Department of Medicine, Division of Gastroenterology, University of California San Diego, 9500 Gilman Drive, Medical Teaching Facility Building, Room 414, La Jolla, CA 92093. E-mail address: vckumar@ucsd.edu

The online version of this article contains supplemental material.

Abbreviations used in this article: B6, C57BL/6; BD, BD Biosciences; CDAA, choline-deficient L-amino acid–defined; cDC, conventional DC; CTGF, connective tissue growth factor; DC, dendritic cell; DT, diphtheria toxin; αGalCer, α-galactosylceramide; HFD, high-fat diet; HSC, hepatic stellate cell; iNKT, invariant NKT; KC, Kupffer cell; MAIT, mucosal-associated invariant T; mDC, myeloid DC; MFI, mean fluorescence intensity; MNC, mononuclear cell; Mo, monocyte; MPO, myeloperoxidase; mtDNA, mitochondrial DNA; NAFL, nonalcoholic fatty liver; NAFLD, nonalcoholic fatty liver disease; NASH, nonalcoholic steatohepatitis; PCoA, principal coordinates analysis; PD, phylogenetic diversity; pDC, plasmacytoid dendritic cell; PERMANOVA, permutational multivariate ANOVA; α-SMA, α-smooth muscle actin; sOTU, sub–Operational Taxonomic Unit picking method; Tg, transgenic; UCSD, University of California San Diego.

NKT cell subsets are predominantly NK1.1$^+$ in mouse or CD161$^+$/CD56$^+$ in human, they also share common features in their TCR repertoire (10, 11). Murine iNKT cells express an invariant germline encoded Vα14/Jα18 TCRα-chain paired with a more diverse nongermline TCRβ-chains, including Vβ8.2, Vβ7, and Vβ2, and human iNKT cells express an invariant Vα24/Jα18 paired predominantly with Vβ11. In contrast, type II NKT cells express a relatively more diverse TCR repertoire and appear to be regulatory in nature. Although the semi-invariant TCR in iNKT cells binds to CD1d in a parallel configuration that mainly involves the α-chain, a type II NKT cell TCR contacts its ligand primarily via its β-chain rather than α-chain, suggesting that the TCR Vβ-chain contributes significantly to Ag fine specificity of type II NKT cells (12). Thus, type II NKT cells use features of TCR binding shared by both iNKT cells and conventional T cells (12, 13). Therefore, both NKT cell subsets display distinct modes of Ag recognition.

One major caveat of the study of NKT cells in inflammatory liver diseases relates to the lack of specific reagents to distinguish between the two major NKT cell subsets and between NKT cells and CD3$^+$CD56$^+$/CD161$^+$ conventional T cells. The most widely used approach involves using the ability of the iNKT cells to recognize the marine sponge–derived glycolipid, α-galactosylceramide (αGalCer) that forms stable CD1d tetramers to identify this subset. For type II NKT cells, there is no universal Ag marker, but we have identified a major subset of type II NKT cells that recognizes a self-glycolipid, sulfatide (13, 14). Thus, quantification of iNKT cells using αGalCer/CD1d tetramers or type II NKT cells using sulfatide or lysophosphatidylcholine/CD1d tetramers, respectively, is crucial to identify each subset and to distinguish them from conventional T cells. For human iNKT cells, a clonotypic Ab (clone 6B11) directed against the human iNKT cell TCR can be used to differentiate them from other T cells (15). We have demonstrated that iNKT cells play a pathogenic role in Ischemia reperfusion injury, Con A–induced hepatitis, and Lieber–DeCarli liquid alcohol diet–induced liver injury, whereas the activation of type II NKT cells following administration with sulfatide or lysophosphatidylcholine induces a dominant anti-inflammatory pathway that prevents liver disease (16–19).

It has been shown that chronic feeding of choline-deficient L-amino acid–defined (CDAA) diet results in steatosis and perisinusoidal/pericellular fibrosis, resembling NASH in humans (20–22). Interestingly, most of the United States population does not meet the recommended intake of choline, and its deficiency is known to exacerbate NAFL and NASH (23–25). In addition, humans with inadequate choline intake have oxidative damage caused by mitochondrial dysfunction and endoplasmic reticulum stress (23). Therefore, it remains unknown whether and/or how different NKT cell subsets can influence the progression from steatosis to fibrosis in a murine model of NASH and in humans. Although recent studies have suggested a potential pathogenic role for NKT cells in diet-induced liver steatosis and fibrosis (26–29), a detailed study of the role of different cytokine-secreting NKT cell subsets and related immune mechanism is lacking.

In this study, we sought to investigate the role of iNKT cell subsets in the development of NASH in a murine model following CDAA diet as well as in PBMCs from NAFLD patients. Our studies revealed the involvement of a key immune mechanism centered on different subsets of iNKT cells mediating progression from steatosis to fibrosis in experimental murine model as well as its potential role in human NAFLD. Activated IL-17– and IL-22–secreting iNKT cells were dominant in liver during the beginning of the steatosis phase, whereas IFN-γ/IL-4/IL-13–secreting iNKT cells were prevalent later in the disease. In addition, activation of iNKT cells is associated with neutrophils, Kupffer cells (KCs), and CD8$^+$ T cells infiltration and upregulation of several key genes related to inflammation, steatosis, and fibrosis. We also found a similar profile of cytokine secretion by iNKT cells in PBMC from NASH patients and, more importantly, a high frequency of CXCR3$^+$/IFN-γ$^+$ iNKT cells in NASH patients. In addition, we found accumulation of plasmacytoid dendritic cells (pDC) into liver following CDAA diet and similar increase of pDC frequency in peripheral blood of NASH patients. Genetic depletion of pDC in BDCA2-DTR mice results in inhibition of iNKT activation, suggesting their role in activation of iNKT cells. In addition, the significant increase in the frequency of CXCR3$^+$/IFN-γ$^+$ iNKT cells as well as pDC in PBMC from NASH patients compared with healthy controls suggests that they could become potential novel biomarkers in the progression of NASH in humans.

Materials and Methods

Ethics statement

Animal studies were carried out in strict accordance with the recommendations of the Guide for the Care and Use of Laboratory Animals of the National Institutes of Health. The protocols were reviewed and approved by the Institutional Animal Care and Use Committee of the University of California San Diego (UCSD). Human studies were approved by the UCSD Institutional Review Board. Informed consent was obtained from all study subjects before blood collection.

Mice

Seven- to ten-week-old male C57BL/6 (B6) and B6 transgenic mice (CLEC4C-HBEGF)956Cln/J (BDCA2-DTR) (JAX stock no. 014176) mice were purchased from The Jackson Laboratory. CD1d$^{-/-}$ and Jα18$^{-/-}$ mice were originally generated by Van Kaer and Taniguchi (30, 31), respectively, and were kindly provided initially by Dr. M. Kronenberg (La Jolla Institute for Allergy and Immunology, La Jolla, CA). All mice were maintained in specific pathogen-free conditions.

Patients and healthy individuals

The study included 23 diagnosed patients with NAFLD: five patients with NAFL and 18 patients with NASH. In parallel, 19 healthy volunteers with no history of liver pathologic condition were obtained from iXCells Biotechnologies (San Diego, CA). Diagnosis of NAFLD was based on the hepatic biopsies and the severity of tissue damage was evaluated on the basis of NAFLD activity score and fibrosis based on the NAFLD fibrosis risk score at the UCSD NAFLD Translational Research Unit. All patients with NASH had significantly higher NAFLD activity scores and NAFLD fibrosis scores compared with NAFL patients.

Murine NASH model

B6 and Jα18$^{-/-}$ mice were maintained on either a CDAA (20% protein, 35% carbohydrate, and 45% fat, without choline; Dyets, Bethlehem, PA) or a normal diet (29% protein, 58% carbohydrate, and 13% fat; LabDiet, St. Louis, MO) for 20 wk. For time-course studies, B6 mice were fed CDAA diet for 1 wk or 1, 2, 3, or 4 mo. CDAA diet has been extensively shown to induce steatohepatitis and fibrosis, which pathologically replicate the histological features of steatohepatitis and fibrosis observed in human NASH.

Isolation of liver mononuclear cells

To obtain mononuclear cells (MNCs), livers were harvested and pressed through a Falcon 70-μm cell strainer (Corning), and suspended in HyClone High Glucose DMEM Medium (Thermo Fisher Scientific, Whaltham, MA). Liver MNCs were washed, and the cell pellet was resuspended in 35% Percoll solution (GE Healthcare Life Sciences, Marlborough, MA) containing 100 U/ml heparin and centrifuged at 2000 rpm at room temperature for 15 min. The supernatant was carefully removed and erythrocytes were disrupted by RBC Lysis Buffer (MilliporeSigma, Burlington, MA). The cells were washed with DMEM supplemented with 2% of FBS, and isolated liver MNCs cells were counted with a hemocytometer using trypan blue and resuspended in FACS buffer (0.02% sodium azide, 2% FBS in PBS).

Isolation of PBMC

Blood samples were taken by venipuncture into sterile, EDTA tubes. PBMCs were isolated by density gradient centrifugation on Ficoll–Hypaque

(MilliporeSigma) at 2000 rpm at room temperature for 30 min. Interphase cells were removed and washed twice in PBS. The cells were counted with a hemocytometer using Türk solution (MilliporeSigma) and resuspended in FACS buffer (0.1% sodium azide, 1% human AB serum, and 1% FBS in PBS).

Flow cytometry analysis and intracellular staining

Data were collected on a FACSCanto flow cytometer (BD Biosciences [BD], San Diego, CA) at the Flow Cytometry Research Core Facility (Veterans Affairs San Diego Healthcare System, San Diego, CA) and analyzed with FlowJo v10 software (TreeStar, Ashland, OR). Mouse Abs (clones) were as follows: anti-TCRβ (H57-597), anti-CD3 (145-2C11), anti-CD4 (GK1.5), anti-NK1.1 (PK136), anti-F4/80 (BM8), anti-CD45 (30-F11), anti-CD11c (N418), anti-CD45R/B220 (RA3-6B2), anti-CD19 (6D5), anti–I-A/I-E (M5/114.15.2), anti–Siglec H (551), anti-CD317 (mPDCA-1) (927), anti-CD103 (2E7) (from BioLegend, San Diego, CA), anti-CD11b (M1/70), and anti–Ly-6C (AL-21) (from BD). PE-conjugated αGalCer/mCD1d tetramers were generated in our laboratory, as previously described (17). To minimize nonspecific Ab binding, cells were previously incubated with anti-CD16/CD32 (Fc Block, 2.4G2) (BD). For intracellular cytokine staining, liver MNCs were stimulated with PMA (10 ng/ml) and ionomycin (500 ng/ml) (MilliporeSigma) for 6 h with addition of BD GolgiPlug containing brefeldin A at the start of culture. Cells were first stained for cell surface markers, then fixed and permeabilized using Cytofix/Cytoperm buffer and stained with the following fluorochrome-labeled mAbs: anti–IFN-γ (XMG1.2), anti–IL-4 (BVD6-24G2), anti–IL-10 (JES5-16E3), anti–IL-13 (eBio13A), anti–IL-17 (eBio17B7), and anti–IL-22 (IL22JOP) (from eBioscience, San Diego, CA). Human Abs were as follows: anti-CD3 (UCHT1), anti-CD19 (SJ25-C1), anti-CD4 (RPA-T4), anti-CD123 (CD1d42), and anti-CD45 (HI30) from BD; anti–Vα24-Jα18 TCR (6B11) from eBioscience; anti-CXCR3 (49801) from R&D Systems; anti-CD14 (HCD14), anti-CD56 (5.1H11), anti-CD11c (Bu15), anti-CD303 (201A), anti-CD141 (M80), and anti-CD1c (ICRF44) from BioLegend; and LIVE/DEAD Fixable Aqua Dead Cell Stain Kit from Thermo Fisher Scientific. For constitutive detection of cytokines and transcription factors in human iNKT cells, no in vitro stimulation was used; instead, PBMC were stained directly for cell surface markers and then fixed and permeabilized as before and incubated with the following mAbs: anti–IFN-γ (4S.B3), anti–IL-17A (eBio64DEC17), anti–IL-22 (22URTI), anti–IL-10 (JES3-9D7), and anti–T-bet (4B10) from eBioscience; and anti–IL-4 (MP4-25D2) and anti–TNF-α (MAb11) from BD.

Tazarotene treatment

Tazarotene (Tocris Bioscience, Ellisville, MO) was injected i.p. at a dose of 300 μg/mouse twice per week over the same period of CDAA feeding. Control mice were injected with DMSO/PBS. Tazarotene was initially diluted in 10% DMSO at 100 mg/ml and further diluted with PBS prior injection.

In vivo depletion of pDC

BDCA2-DTR mice and littermates were depleted of pDC by injecting 200 ng of diphtheria toxin (DT) (MilliporeSigma) on day −2 and −1 of CDAA diet. Similar DT treatment was made on day 3 and 6 after starting CDAA diet. Mice were sacrificed on day 8 and pDC depletion was verified by flow cytometry.

In vitro PBMC stimulation

PBMCs (2×10^6/well, duplicate) were cultured into 96-well plate in 250 μl of RPMI 1640 medium supplemented with 10% FBS, 1% L-glutamine, 1% penicillin/streptomycin, and 40 U/ml of human rIL-2 (PeproTech, Rocky Hill, NJ) with 100 ng/ml αGalCer or without stimulation. The cells were cultured for 10 d at 37°C in an atmosphere containing 5% CO_2. Supernatants of cell cultures were collected on day 4 and stored at −80°C until cytokine analysis. Cells in culture were harvested on day 10 after stimulation and stained for analysis of iNKT cells by FACS as above. Fold expansion of iNKT cells was calculated by dividing frequencies of iNKT cells in PBMC cultures containing αGalCer during 10-d expansion by the frequencies on day 0 without stimulation. Secretion of cytokines in the supernatants was determined using the BD Cytometric Bead Array Human Th1/Th2/Th17 Cytokine Kit (BD).

Histology

Liver tissues were fixed in 10% formaldehyde solution and kept at room temperature until use. H&E staining of tissue sections (5-μm) was performed at the UCSD Neuroscience Core for Microscopy. Steatosis and liver fibrosis were assessed with Sirius Red/Fast Green staining. Myeloperoxidase (MPO) staining was performed using anti-MPO Ab-1 rabbit polyclonal Ab (Thermo Fisher Scientific). All pictures were taken using the NanoZoomer 2.0-HT Slide Scanning System (Hamamatsu, Japan) and quantitated on ImageJ software (National Institutes of Health).

Microbiome analysis

Stool collection. Three to four fresh fecal pellets were collected individually from mice (each mouse was placed in a confined place to avoid cross-contamination) using sterile cotton swabs into individually labeled sterile 0.6-ml Eppendorf tube. Samples were collected during 2 d from colonies of mice of mixed age and sex that were maintained in our animal facility for a minimum of 2–3 wk to 8 mo. Following collection, tubes containing stool samples were stored at −80°C until analysis. For CDAA diet–fed groups, mice were age and sex matched and fecal pellets were collected similarly but at the end of the experiment.

16S rRNA gene sequencing. DNA was extracted using the PowerSoil DNA Extraction Kit (MO BIO Laboratories) according to Earth Microbiome Project standard protocols (32) (http://www.earthmicrobiome.org/emp-standard-protocols/). PCR targeting the V4 region of the 16S rRNA bacterial gene was performed with the 515F/806R primers, using the protocol described in Walters et al. (33). Amplicons were barcoded and pooled in equal concentrations for sequencing. The amplicon pool was purified with the UltraClean PCR Clean-Up Kit (MO BIO Laboratories), and 2 × 150–bp sequencing was performed on the MiSeq System sequencing platform at the Institute for Genomic Medicine at UCSD.

16 rRNA sequencing data processing and analysis. Raw sequencing data were deposited in Qiita and processed via QIIME v1.9.1 (34) in Qiita using parameters for demultiplexing and quality control recommended by Bokulich et al. (35). Forward reads were trimmed to 150 bp and then processed with deblur (36), a de novo sub–Operational Taxonomic Unit picking method (sOTU). The resulting sOTUs were inserted into the Greengenes tree (37) and assigned taxonomy via SATé-Enabled Phylogenetic Placement using q2-fragment-insertion in QIIME2 (34, 38) (https://qiime2.org). sOTUs were directly visualized in QIIME2 via Faith phylogenetic diversity (PD) (39) and Unweighted and Weighted UniFrac distances (40–42) were computed for each experimental group, and then results were visualized in EMPeror (43, 44). The sequencing data presented in this article have been submitted to the Qiita study (https://qiita.ucsd.edu/study/description/10781).

RNA, DNA, RT-PCR, and real-time PCR analysis

Total RNA was isolated from liver tissues using a PureLink RNA Mini Kit (Ambion, Thermo Fisher Scientific). RNA was quantified using NanoDrop 2000c spectrophotometer (Thermo Fisher Scientific) and reverse transcribed using RevertAid First Strand cDNA Synthesis Kit (Ambion). To detect mRNA of Vα14Jα281 gene, 5 μg of total RNA were reverse transcribed and subjected to a nested PCR as previously described (45) using the following primer pairs: for first-round PCR, Vα14 Leader, 5′-ATGAAAAAGCGCCTGAGTGCC-3′, C-rev1 reverse, 5′-CAGGAGGATTCGGAGTCCCA-3′; for nested PCR, Vα14/Jα281, forward, 5-TAAGCACAGCACGTGCACAT-3′, Vα14/Jα281, reverse, 5′-CAATCAGCTGAGTCCCAGCT-3′. Real-time PCR was performed using KAPA SYBR Fast Master Mix (Thermo Fisher Scientific) on a StepOnePlus Real-Time PCR System (Applied Biosystems) with specific PCR primer pairs. Data were analyzed using the ΔΔ cycle threshold method against normal diet–fed wild type mice. Genomic DNA was extracted from the tail of BDCA2-DTR mice's littermates using DNeasy Blood & Tissue Kit (Qiagen) and subjected to PCR following The Jackson Laboratory protocol [transgenic mice (CLEC4C-HBEGF)].

Western blot

Whole cell lysates of liver (50 μg) were separated on a gradient (4–20%) polyacrylamide NuPAGE gel (Thermo Fisher Scientific) and transferred onto nitrocellulose membranes and blotted with anti–α-smooth muscle actin (α-SMA) mAb (GeneTex, Irvine, CA) or anti–β-actin (Santa Cruz, Dallas, TX). Proteins were detected with peroxidase-conjugated secondary Ab. Protein bands were visualized using an ECL reagent and digitized using ChemiDoc Imaging System (Bio-Rad Laboratories). Expression intensity was quantified by Image Lab.

Statistical analyses

Data were analyzed using GraphPad Prism v7 software (GraphPad Software). For all analyses, data were presented as mean ± SEM. For comparison between two groups, unpaired *t* test for mouse data or two-tailed Mann–Whitney *U* test for human data were applied. For comparison between three groups (i.e., frequency of iNKT as well as cytokine secretion or transcription factor expression in human PBMCs), one-way ANOVA with Tukey correction was applied. For all analyses, *p* values were indicated as follows: $*p \leq 0.05$, $**p \leq 0.01$, $***p \leq 0.001$, and $****p \leq 0.0001$.

Results

Activation and differential cytokine secretion profiles of iNKT cells in a diet-induced NASH model

Because chronic feeding of CDAA diet results in liver damage resembling NASH in humans (20–22), we investigated whether progression of diet-induced steatosis to fibrosis is associated with the alterations in the cytokine secretion profile of iNKT cells in liver. Liver MNCs derived from B6 mice maintained on standard normal diet or CDAA diet for 1 wk or 1, 2, 3, or 4 mo were analyzed using αGalCer/CD1d tetramers and intracellular cytokine-based flow cytometry approach. The results showed that IL-17$^+$– and IL-22$^+$–iNKT cells (NKT17) as well as IL-10$^+$–iNKT cells (NKT10) (TCRβ$^+$NK1.1$^+$αGalCer/CD1d-tet$^+$) increased significantly during progression of steatosis, reaching a peak at 3 mo of CDAA diet as compared with normal diet–fed B6 mice (Fig. 1A, Supplemental Fig. 1). However, there was no significant increase in IL-17$^+$– and IL-22$^+$–conventional T cells (TCRβ$^+$NK1.1$^+$αGalCer/CD1d-tet$^-$) at these time points (Supplemental Fig. 2). Interestingly, IFN-γ$^+$–, IL-4$^+$–, and IL-13$^+$–iNKT cells (NKT1/NKT2) increased significantly much later during steatosis/fibrosis compared with mice fed normal diet (Fig. 1A, Supplemental Fig. 1). At this later stage following CDAA diet, even conventional T cells significantly produced IFN-γ, but not IL-4 (Supplemental Fig. 2). In summary, the cytokine secretion profile of iNKT cells skewed from predominantly NKT17- to NKT1/NKT2-like, and it correlates with the progression from steatosis to fibrosis following CDAA diet.

Because iNKT cells can downregulate their TCR following chronic stimulation, we compared hepatic iNKT cells between B6 mice fed CDAA diet versus normal diet using αGalCer/CD1d tetramer staining. The results revealed a significant decrease in the tetramer staining of iNKT cells in mice fed CDAA diet compared with normal diet–fed mice (Fig. 1B). We next investigated whether chronic activation of iNKT cells also leads to downregulation of cell surface expression of NK1.1 in addition to TCR. As shown in Fig. 1C, NK1.1 expression was also significantly downregulated in iNKT cells after CDAA diet in comparison with the normal diet. To further examine that the reduced tetramer staining results from TCR downmodulation, but not from deletion of iNKT cells following chronic activation, we used a semiquantitative RT-PCR approach to analyze the Vα14-Jα18 TCR transcript expression. As expected, the relative quantity of hepatic Vα14-Jα18 PCR product was not decreased, but significantly increased in mice fed CDAA diet compared with normal diet–fed mice (Fig. 1D). Collectively, our data indicate that chronic activation of hepatic iNKT cells is associated with cytokine profile changes and downregulation of both cell surface NK1.1 and invariant TCR during CDAA diet–induced hepatic steatosis and fibrosis.

iNKT cell–deficient Jα18$^{-/-}$ mice are protected from diet-induced hepatic steatosis and fibrosis

To further investigate the role of iNKT cells in the pathogenesis of NASH, iNKT cell–deficient Jα18$^{-/-}$ and B6 mice were fed normal diet or CDAA diet. As shown in Fig. 2A, CDAA diet significantly increased body and liver weight in both B6 and Jα18$^{-/-}$ mice compared with normal diet. Liver weight was significantly reduced in Jα18$^{-/-}$ mice compared with B6 mice. But, epididymal adipose tissue weight did not differ significantly between B6 and Jα18$^{-/-}$ mice following CDAA diet. However, alanine aminotransferase levels and triglycerides were significantly reduced in Jα18$^{-/-}$ liver compared with B6 mice (Fig. 2B). More importantly, CDAA diet resulted in significant liver damage as indicated by marked steatosis, hepatocyte ballooning, and collagen deposition compared with normal diet–fed B6 mice (Fig. 2C), but Jα18$^{-/-}$ mice had significantly less liver damage than B6 mice. These results indicate that mice lacking iNKT cells (Jα18$^{-/-}$) were significantly protected from steatosis and fibrosis following CDAA diet, suggesting a pathogenic role of iNKT cells in NASH progression in mice.

To determine whether hepatic stellate cell (HSC) activation is also influenced by iNKT cells following CDAA diet, we assessed α-SMA expression by immunohistochemistry in liver sections from CDAA-fed B6 and Jα18$^{-/-}$ mice. Our results show that α-SMA–positive areas were significantly reduced in Jα18$^{-/-}$ liver compared with B6 (Fig. 2D). Consistent with this, α-SMA expression levels, measured via α-SMA Western blot, were also reduced in Jα18$^{-/-}$ liver compared with B6 following CDAA diet (Fig. 2E). Accordingly, quantitative real-time RT-PCR analyses confirmed that α-SMA transcripts were significantly reduced in Jα18$^{-/-}$ liver compared with B6 mice (Fig. 2F). Furthermore, other key fibrogenic genes like TIMP-1, collagen (COL1) and connective tissue growth factor (CTGF) showed significantly reduced expression in CDAA-fed Jα18$^{-/-}$ mice in comparison with B6 mice (Fig. 2F). These results indicate a key role for iNKT cells in diet-induced HSC activation, steatosis, and fibrosis in liver.

Reduced liver inflammation in Jα18$^{-/-}$ mice following CDAA diet

Next, we examined whether hepatic inflammatory pathways are involved in protecting Jα18$^{-/-}$ mice from diet-induced steatosis and fibrosis. Indeed, CDAA feeding of Jα18$^{-/-}$ mice resulted in a significant reduction of hepatic neutrophil infiltration, analyzed by MPO staining compared with CDAA-fed B6 mice (Fig. 3A). Moreover, the expression level of several key inflammatory genes, including TNF-α, IL-6, KC, and MIP-2, as well as genes related to inflammasome activation like NLRP3 and IL-1β was significantly reduced in Jα18$^{-/-}$ liver compared with B6 following CDAA diet (Fig. 3B). However, genes involved in gluconeogenesis or lipid metabolism did not differ between Jα18$^{-/-}$ and B6 mice following CDAA diet except for downregulation of PEPCK in Jα18$^{-/-}$ mice (Fig. 3B). These results suggest that diet-induced liver inflammation and steatohepatitis are reduced in the absence of iNKT cells, confirming their critical role in mediating diet-induced NASH.

A RAR-γ agonist treatment inhibits effector function of iNKT cells and protects mice from CDAA-induced steatosis and fibrosis

We have recently shown that an agonist of the RAR-γ, tazarotene, specifically inhibits iNKT cells, but not type II NKT cells or conventional T cells, and significantly protects mice from alcoholic liver disease and carbon tetrachloride (CCL4)–induced fibrosis (18). To determine whether functional inhibition of iNKT cells protects mice from diet-induced liver injury, CDAA-fed B6 mice were treated twice a week i.p. with tazarotene (300 μg/mouse) or DMSO/PBS. As shown in Fig. 4A, tazarotene treatment significantly blunted CDAA-induced increase in body, liver, and epididymal adipose tissue weight as compared with untreated mice. More importantly, tazarotene treatment significantly reduced steatosis, collagen deposition, and HSC activation following CDAA diet (Fig. 4B). Next, we investigated whether suppression of liver disease results from the inhibition of iNKT cells in tazarotene-treated animals. We determined the function of iNKT cells in both control and treated groups of mice by measuring proliferative response and cytokine secretion after in vitro stimulation with αGalCer. As shown in Fig. 4C, both proliferation and cytokine secretion by iNKT cells were significantly inhibited following tazarotene treatment. Additionally, we found that functional inhibition of iNKT cells was not consequence of reduced numbers of iNKT cells in tazarotene-treated mice as shown by similar

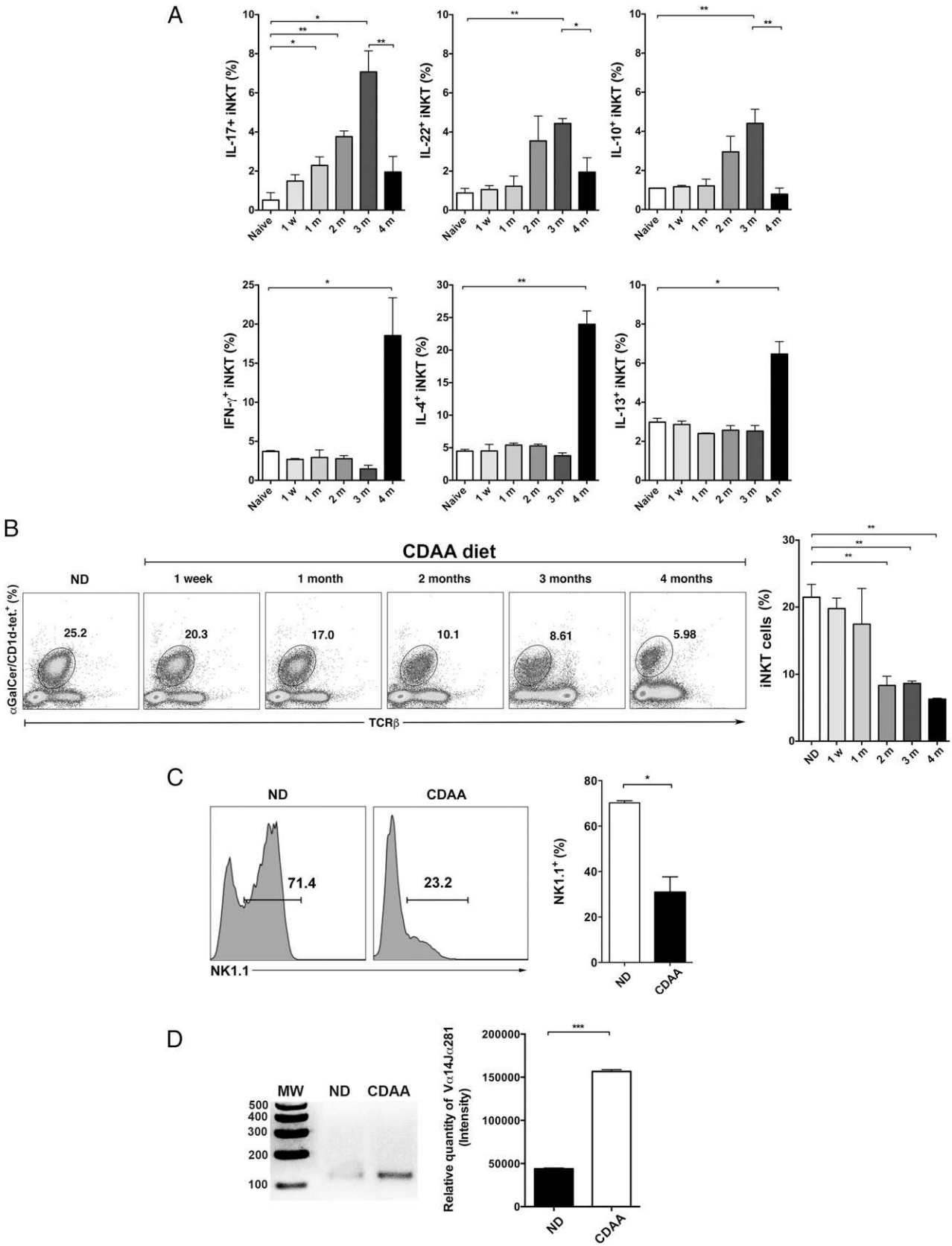

FIGURE 1. Differential activation and cytokine secretion profiles of hepatic iNKT cells in a diet-induced NASH model. (**A**) Wild type B6 mice were maintained on standard normal diet (ND) or were fed CDAA diet for 1 wk or 1, 2, 3, or 4 mo. Liver MNCs from each experimental group were stimulated in vitro with PMA and ionomycin for 6 h in the presence of GolgiPlug. Cells were stained with anti-TCRβ, anti-NK1.1, and αGalCer/CD1d tetramer before they were fixed, permeabilized, and stained with anti–IFN-γ, anti–IL-17, anti–IL-22, anti–IL-10, anti–IL-4, and anti–IL-13 mAbs. iNKT cells were identified as double TCRβ- and αGalCer/mCD1d tetramer–positive cells (TCRβ$^+$/αGalCer/mCD1d tetramer$^+$) in the NK1.1$^+$ gate. Cytokine-secreting cells were gated on iNKT cells. Bar graphs show the percentage of iNKT cells secreting IFN-γ, IL-17, IL-4, IL-10, IL-13, and IL-22 in liver of ND- or CDAA diet–fed B6 mice for the indicated time points. Each group included three mice. (**B**) Representative dot plots of iNKT cells in *(Figure legend continues)*

numbers of αGalCer/CD1d-tetramer$^+$ cells and Vα14-Jα18 PCR products in livers of both groups of animals (Fig. 4D). Overall, these data are consistent with the data shown in CDAA-fed Jα18$^{-/-}$ mice. Thus, both genetic deficiency as well as functional inhibition of iNKT cells leads to the inhibition of diet-induced hepatic steatosis and fibrosis.

Hepatic infiltration by CD8$^+$ T cells and macrophages following CDAA diet is dependent on iNKT cells

Recent data have suggested an important role of hepatic CD8$^+$ T cells and KCs in murine models of steatosis and fibrosis (28, 46, 47). Next, we determined the role of iNKT cells in hepatic infiltration of CD8$^+$ T cells in diet-induced liver disease. As expected, CDAA diet significantly increased the frequency of CD8$^+$ T cells in liver MNCs compared with normal diet (Fig. 5A). We found that the hepatic infiltration of CD8$^+$ T cells in CDAA-induced liver damage was significantly decreased in Jα18$^{-/-}$ mice as compared with B6 mice (Fig. 5A).

Because inflammatory macrophages also play a significant role in liver injury, we investigated whether CDAA diet promoted hepatic macrophage infiltration. We followed three distinct subsets of proinflammatory macrophages within liver: KCs, monocytes (Mos), and Mo-derived macrophages gated on CD45$^+$F4/80$^+$ cells as described before (48). Indeed, the frequency of hepatic KC was significantly increased in CDAA-fed B6 mice compared with normal diet–fed B6 mice (Fig. 5B); however, the frequency of Mos and Mo-derived macrophages did not differ between B6 mice feeding CDAA diet or normal diet (Fig. 5B).

To further confirm that the effects on CD8$^+$ T cells and KC mediated by CDAA diet were dependent on functional iNKT cells, B6 mice maintained on CDAA diet for 20 wk were treated with tazarotene (300 μg/mouse) as before. Tazarotene treatment significantly reduced the frequency of both CD8$^+$ T cells and KC in liver of CDAA-fed B6 mice as compared with untreated mice (Fig. 5C). These results confirm the key role of iNKT cells in mediating liver infiltration by CD8$^+$ T cells and KC, consistent with our results in CDAA-fed Jα18$^{-/-}$ mice.

iNKT cells from NASH patients are activated and secrete proinflammatory cytokines

We next sought to determine whether there was evidence of a similar change in the frequency and cytokine profile of circulating iNKT cells in patients with NAFLD as we observed in the murine model of NASH. We first compared the frequency of iNKT cells in peripheral blood between patients with NAFLD (five patients with NAFL and 18 patients with NASH) and 19 healthy controls using a mAb that recognize the invariant CDR3 loop of the human canonical Vα24Jα18 TCR α-chain (clone 6B11) (15) in a multiparameter flow cytometry approach to specifically identify human iNKT cells (Fig. 6A). The selective labeling of iNKT cells was validated by αGalCer/human CD1d tetramer staining that shows equivalent frequencies (data not shown). The frequency of circulating iNKT cells was not significantly different between groups. However, NASH patients exhibited high frequency of circulating iNKT cells (0.34 ± 0.18% versus 0.1 ± 0.03% in healthy controls and versus 0.08 ± 0.05% in NAFL patients) (Fig. 6B). We next examined the functionality of iNKT cells in NAFLD patients and healthy controls by measuring the spontaneous production of IFN-γ, IL-4, IL-17A, IL-22, IL-10, and TNF-α as well as the expression of CXCR3 and T-bet. Compared with both NAFL patients and healthy controls, iNKT cells from NASH patients secreted significantly more IFN-γ, as measured by geometric mean fluorescence intensity (MFI; 679.4 ± 130.1 versus 183.2 ± 30.1 in healthy controls and versus 171.3 ± 69.3 in NAFL patients), than NAFL patients and healthy controls (Fig. 6C, first panel). This was consistent with the analysis of the transcription factor T-bet, which was also highly expressed by iNKT cells from NASH patients compared with healthy control (MFI: 9763 ± 2017 versus 2458 ± 330.3 in healthy controls) (Fig. 6C, second panel). Consistent with a proinflammatory profile, iNKT cells from NASH patients expressed significantly more CXCR3 compared with iNKT cells from both NAFL patients and healthy controls (MFI: 1422 ± 194.4 versus 559.4 ± 74.6 in healthy controls and versus 550.8 ± 59.1 in NAFL patients) (Fig. 6C, third panel). IL-4 secretion was not significantly different in iNKT cells from NASH or NAFL patients and healthy controls (Fig. 6C, last panel). Furthermore, 55% of NASH patients (10 out of 18) had a population of iNKT cells that produce more IFN-γ than IL-4 ($p < 0.001$, Fisher test), whereas 87.5% of healthy controls (14 out of 16) had a population of iNKT cells that constitutively secrete more IL-4 than IFN-γ ($p = 0.0083$, Fisher test) (data not shown).

Additionally, iNKT cells from NASH patients significantly secreted more IL-17A compared with healthy controls (MFI: 293.6 ± 116.6 versus 108.1 ± 20.9) (Fig. 6D). However, when the level of liver fibrosis was considered, patients with advance fibrosis (Fibrosis score 2–4) had lower levels of IL-17A and higher levels of IFN-γ compared with patients with fibrosis score ≤1 (data not shown). Moreover, iNKT cells from NASH patients secreted similar amounts of IL-22, TNF-α, and IL-10 compared with iNKT cells from healthy controls (Fig. 6D). These data suggest that iNKT cells from NASH patients are more activated and proinflammatory as defined by higher expression of CXCR3, T-bet, IL-17A, and IFN-γ.

It is interesting that conventional CD3$^+$CD4$^+$ T cells were significantly increased in peripheral blood of NASH patients compared with healthy controls (67.6 ± 2.6% versus 59.6 ± 2.2%), and consequently, the CD4$^+$/CD8$^+$ ratio was also significantly increased in NASH patients; however, the frequency of CD8$^+$ T cells was not different between NASH patients and healthy controls. NAFL patients showed similar trend as NASH patients, but the difference did not reach statistical significance (data not shown).

Interestingly, we detected a subset of iNKT cells that coexpress IFN-γ and CXCR3 (IFN-γ$^+$CXCR3$^+$ iNKT cells) significantly increased in NASH patients compared with healthy controls (47.64 ± 4.73% versus 18.78 ± 3.2%) (Fig. 6E). Also, IFN-γ$^+$CXCR3$^+$ iNKT cells were significantly increased in NASH patients, but not in healthy controls, compared with IFN-γ$^+$CXCR3$^+$ conventional CD3$^+$ T cells (CD3$^+$Vα24Jα18TCR$^-$) (47.64 ± 4.73% versus 27.15 ± 2.61%) (Fig. 6E). These results indicate that IFN-γ$^+$CXCR3$^+$

liver of mice as indicated in (A). Numbers on dot plots indicate the percentage of αGalCer/CD1d tetramer$^+$ TCRβ$^+$ cells within the drawn gate. Bar graph shows the percentage of tetramer$^+$ cells in liver of mice as indicated in (A). (**C**) Histograms show representative NK1.1 expression on gated tetramer$^+$ cells as indicated in (A) in liver of B6 mice fed ND or CDAA diet. Bar graph shows the percentage of NK1.1$^+$ cells gated on αGalCer/CD1d tetramer$^+$ TCRβ$^+$ cells. (**D**) Representative gel of Vα14Jα18 mRNA expression in liver of B6 mice fed ND or CDAA diet for 3 mo, as determined by nested PCR. Jα18$^{-/-}$ mice were used as negative control. Bar graph shows the relative quantity of PCR product liver of B6 mice fed ND ($n = 2$) or CDAA diet for 3 mo ($n = 3$) All data are presented as mean ± SEM. Data representative of three independent experiments. *$p < 0.05$, **$p \leq 0.01$, ***$p \leq 0.001$ by unpaired two-sample *t* test.

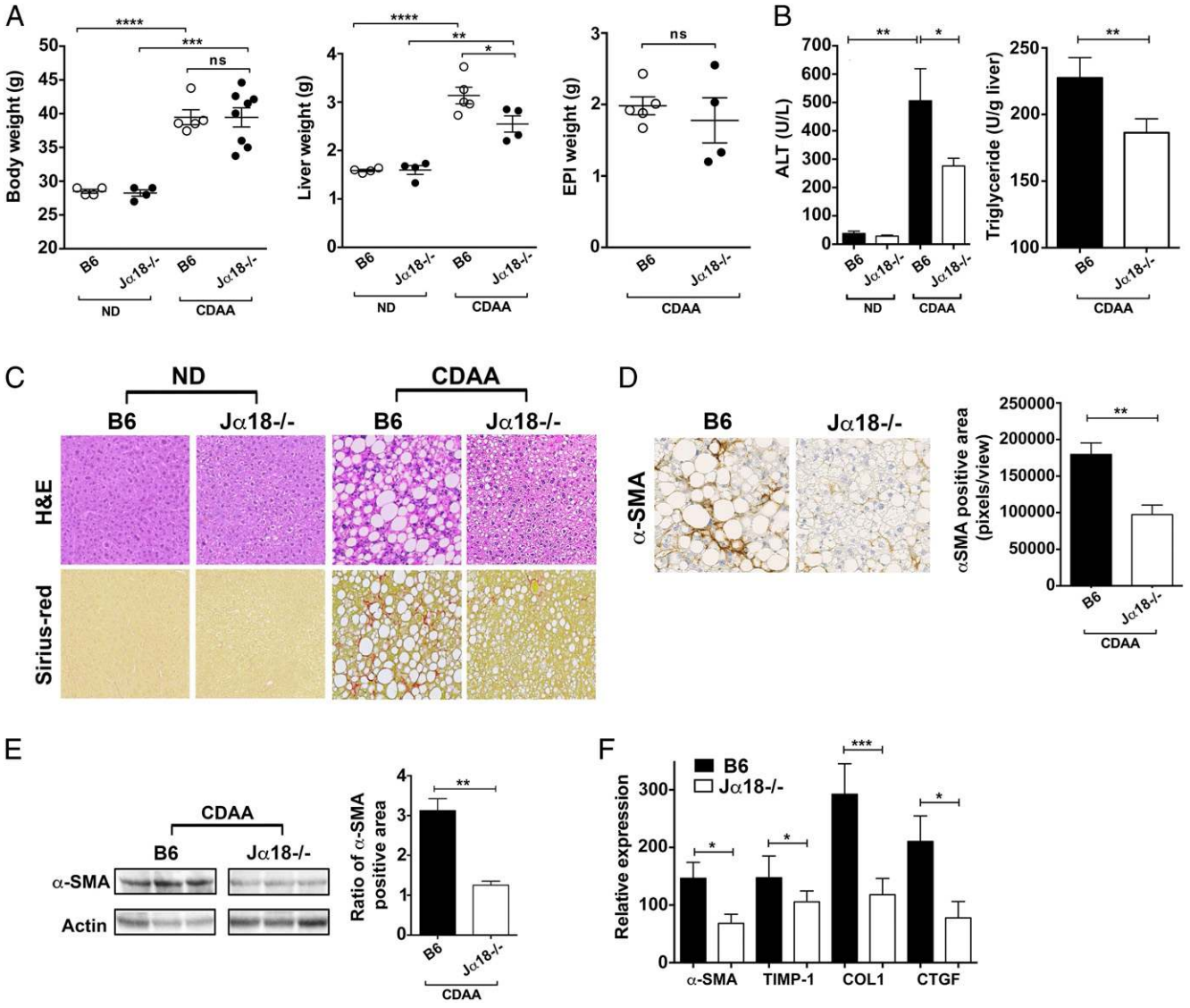

FIGURE 2. iNKT cell–deficient J$\alpha18^{-/-}$ mice are protected from diet-induced hepatic steatosis and fibrosis. B6 and J$\alpha18^{-/-}$ mice were fed normal diet (ND) or CDAA diet for 20 wk. (**A**) Body, liver, and epididymal adipose tissue weight of B6 and J$\alpha18^{-/-}$ mice following ND or CDAA diet are shown. Each point represents an individual mouse of at least four mice in each group. (**B**) Bar graphs show the alanine aminotransferase (ALT) levels in the serum of B6 and J$\alpha18^{-/-}$ mice following ND or CDAA diet (left) and triglycerides levels in liver of CDAA-fed B6 and J$\alpha18^{-/-}$ mice. Each group included five mice. (**C**) Representative H&E and Sirius Red staining of liver sections from B6 and J$\alpha18^{-/-}$ mice fed ND or CDAA diet. Photomicrographs were prepared at original magnification ×100. (**D**) Representative immunohistochemistry staining for α-SMA in liver sections from B6 and J$\alpha18^{-/-}$ mice following CDAA diet. Photomicrographs were prepared at original magnification ×100. Bar graph shows the quantification of α-SMA–positive areas in the indicated groups. Each group included five mice. (**E**) Representative Western blot of α-SMA protein expression in liver homogenates from B6 and J$\alpha18^{-/-}$ mice fed CDAA diet. Bar graph shows the quantification of the ratio of α-SMA–positive area in the indicated groups. Each group included five mice. (**F**) Bar graph shows the relative expression of selected fibrogenic genes in liver tissue from B6 and J$\alpha18^{-/-}$ mice following CDAA diet as determined by quantitative RT-PCR. The expression of each gene was normalized using a reference control gene and its relative expression calculated considering the expression levels in ND-fed B6 mice. Each group included four to seven mice. All data are presented as mean ± SEM. Data representative of three independent experiments. $*p < 0.05$, $**p \leq 0.01$, $***p \leq 0.001$, $****p \leq 0.0001$ by unpaired two-sample *t* test.

iNKT cells were more prevalent in NASH patients than in healthy controls.

iNKT cells in NASH patients are chronically activated and hyporesponsive to in vitro stimulation with αGalCer

Because iNKT cells following chronic activation in vivo can become refractory to subsequent ex vivo stimulation, we determined their ex vivo response to αGalCer in PBMC from NASH patients and compared with those from healthy controls. As shown in Fig. 7A, iNKT cells expansion was significantly decreased in NASH patients. The fold expansion of iNKT cells in the cultures was significantly reduced in NASH patients (25.6 ± 8.5) compared with healthy controls (93 ± 39.3) (Fig. 7B). Consistent with their hyporesponsiveness, the secretion of several cytokines, including IL-6, IFN-γ, IL-17A, and IL-4, after αGalCer stimulation was also significantly reduced in NASH patients compared with healthy controls (Fig. 7C). Collectively, these data further indicate chronic in vivo activation of iNKT cells in NASH progression.

Dendritic cell subsets are altered and involved in iNKT activation in both murine and human NASH

Because the liver is enriched in different dendritic cell (DC) subsets that can play a central role in iNKT cell activation, we determined whether they are involved in progression of NASH in a murine

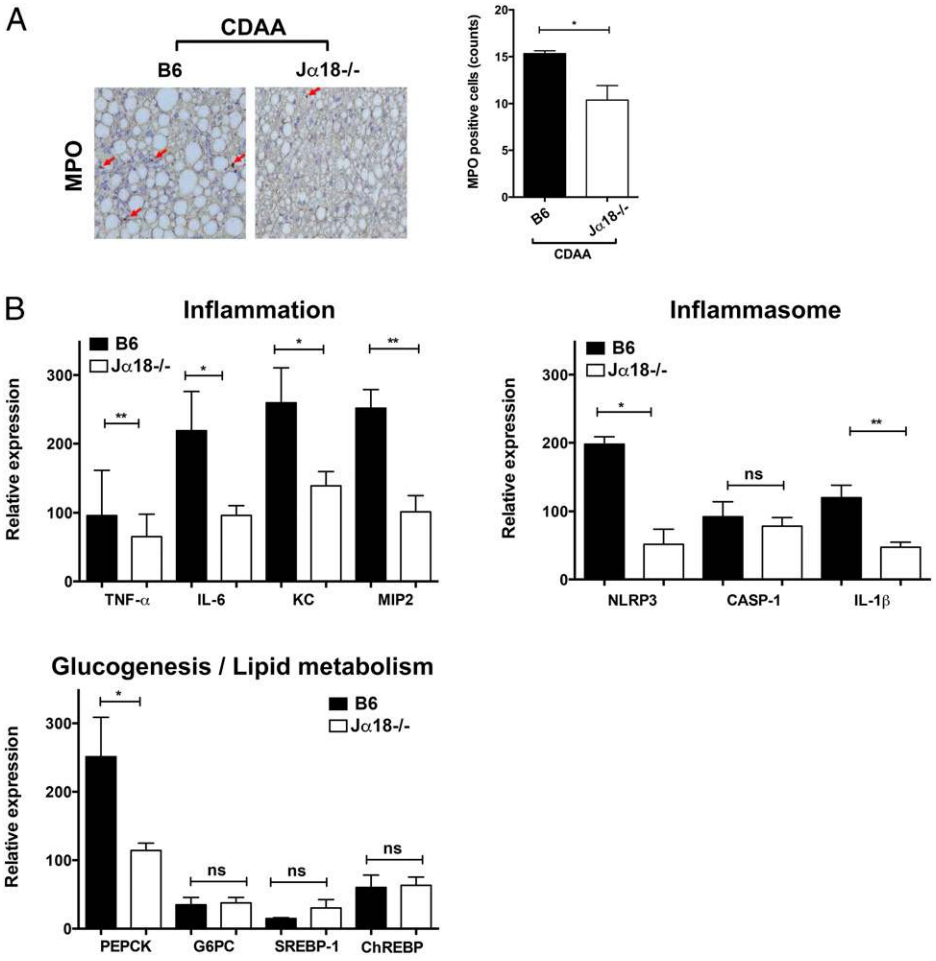

FIGURE 3. Reduced liver inflammation in iNKT cell–deficient Jα18$^{-/-}$ mice following CDAA diet. B6 and Jα18$^{-/-}$ mice were fed normal diet or CDAA diet for 20 wk. (**A**) Representative immunohistochemistry staining for MPO in liver sections of B6 and Jα18$^{-/-}$ mice following CDAA diet. Photomicrographs were prepared at original magnification ×100. Bar graph shows the quantification of MPO-positive cells in the indicated groups. Each group included four mice. (**B**) Bar graphs show the relative expression of selected genes in liver tissues from B6 and Jα18$^{-/-}$ mice following CDAA diet as determined by quantitative RT-PCR. The expression of each gene was normalized using a reference control gene and its relative expression calculated considering the expression levels in normal diet–fed B6 mice. Each group included five mice. All data are presented as mean ± SEM. Data representative of three independent experiments. $*p < 0.05$, $**p \leq 0.01$ by unpaired two-sample *t* test.

model and in NASH patients. We first examined the frequency of pDC (PDCA-1$^+$SiglecH$^+$) and two major subsets of conventional DCs (cDCs), CD103$^+$ cDC (CD103$^+$CD11b$^-$) and CD11b$^+$ cDC (CD103$^-$CD11b$^+$), in liver MNCs from B6 mice fed CDAA diet. Interestingly, the pDC population was significantly increased in liver of mice fed CDAA diet compared with normal diet–fed B6 mice (Fig. 8A). In contrast, CD103$^+$ cDC were significantly decreased in CDAA-fed mice compared with normal diet–fed mice, whereas CD11b$^+$ cDC were not affected significantly (Fig. 8B). These changes suggest that DC subsets infiltrate into liver differentially during CDAA diet-induced liver injury. Importantly, CD1d surface expression on pDC was similar between B6 mice fed CDAA or normal diet (Fig. 8C). Next, we investigated whether pDC infiltration into liver influenced the activation of hepatic iNKT cells following CDAA diet. To examine pDC role in downregulation of αGalCer/CD1d tetramer$^+$ iNKT cells, we used transgenic BDCA2-DTR mice, in which pDCs can be specifically depleted with DT. Thus, BDCA2-DTR mice and littermates (transgene negative) were injected with DT as described, and liver MNCs were analyzed by FACS. We found that DT-induced pDC depletion resulted in a significant inhibition of the downregulation of tetramer$^+$ cells in BDCA2-DTR mice, but not in littermates, following CDAA diet (Fig. 8D). These results indicate that pDC play an important role in CDAA-induced activation and iNKT TCR downregulation.

Next, we determined whether the DCs populations are also affected in NASH patients and whether there is any similarity with the murine data. Therefore, we analyzed the frequency in peripheral blood of NASH patients and healthy controls of pDC (CD123$^+$CD11c$^-$) and two subsets of myeloid DCs (mDCs): CD141^{high} mDC, which seem to be the human counterpart of mouse CD103$^+$ cDC, and CD1c$^+$ mDC, which appear to be related to mouse CD11b$^+$ cDC (Fig. 8E). Consistent with our data in murine model of NASH, the pDC population was significantly increased in peripheral blood from NASH patients compared with healthy controls (11.44 ± 2.08% versus 3.86 ± 1.17%) (Fig. 8E, bottom). In contrast, the frequency of CD141^{high} (1.05 ± 0.22% versus 2.1 ± 0.31%) and CD1c$^+$ (13.46 ± 2.58% versus 28.5 ± 5.53%) mDCs was significantly reduced in NASH patients compared with healthy controls (Fig. 8E, bottom). These results indicate that these pDC and mDC subsets are altered in peripheral blood of NASH patients and may play a role in NASH.

Altered gut microbiota in Jα18$^{-/-}$ mice and CDAA diet–fed mice

Previous reports have suggested that gut microbiota could potentially have an impact on inflammation in NAFLD (49, 50); we next analyzed the V4 region of the 16S rRNA genes (32) in stool samples to assess whether the protection in iNKT cell–deficient mice (Jα18$^{-/-}$) is related to the differences in microbial diversity. Because the microbiome in Jα18$^{-/-}$ and CDAA-treated mice was unknown, we performed a detailed characterization of the composition in our experiments. We found significant differences in the composition of the community between Jα18$^{-/-}$ and B6 mice, with greatly increased α diversity in Jα18$^{-/-}$ mice as measured by Faith PD (Kruskal–Wallis $q = 9.28 \times 10^{-7}$, Fig. 9A) (39). In addition, both strains showed significant and dramatic separation in principal coordinates analysis (PCoA) space of unweighted

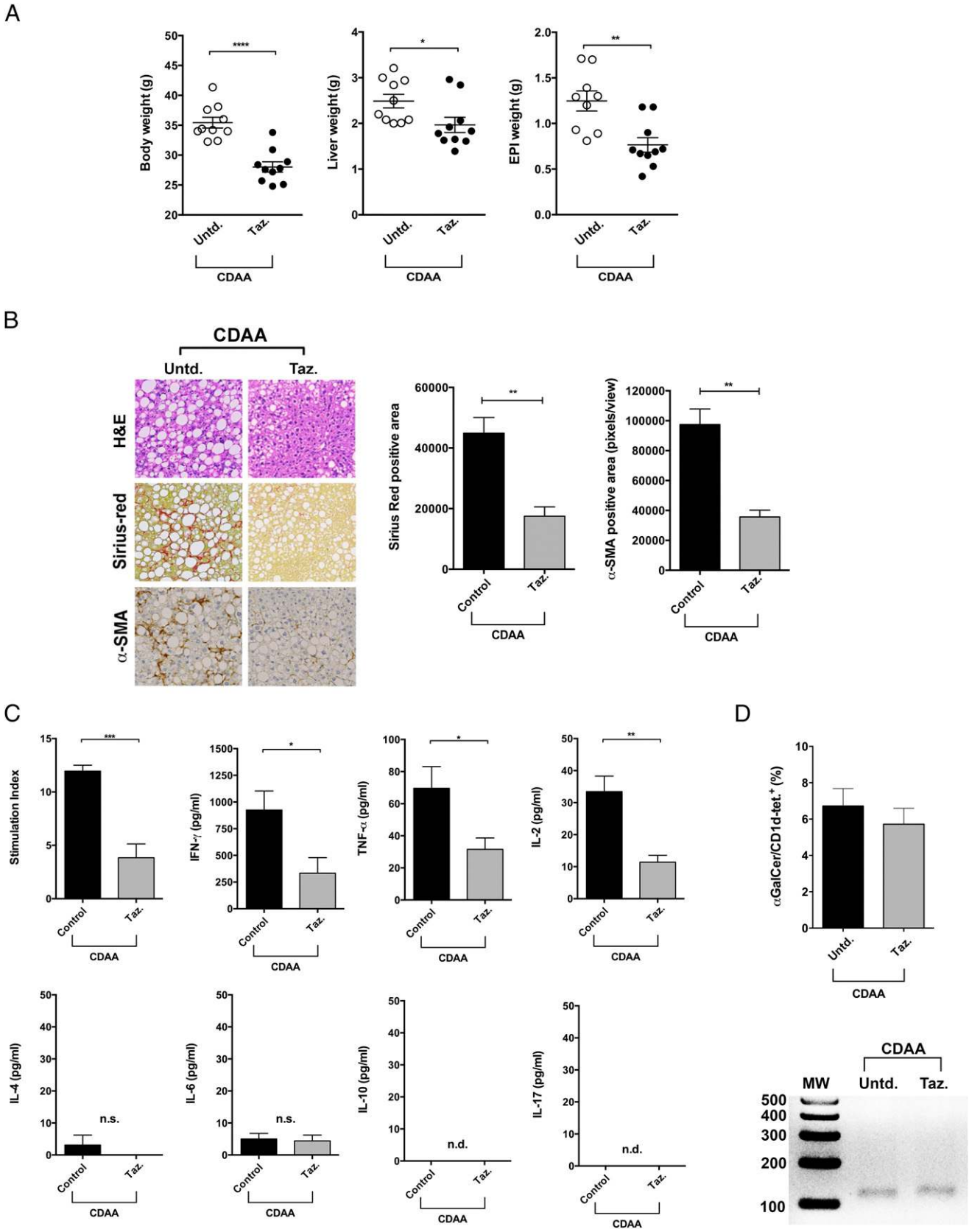

FIGURE 4. Treatment of B6 mice with a RAR-γ agonist inhibits effector function of iNKT cells and protects mice from CDAA-induced steatosis and fibrosis. B6 mice maintained on CDAA diet for 20 wk were subjected to i.p. injection of tazarotene (300 μg/mouse) twice per week or left untreated. (**A**) Body, liver, and epididymal adipose tissue weight in B6 mice untreated or treated with tazarotene following CDAA diet are shown. Each point represents an individual mouse. Each group included 10 mice. (**B**) Representative H&E, Sirius Red and α-SMA staining of liver sections from CDAA-fed B6 mice untreated or treated with tazarotene. Photomicrographs were prepared at original magnification ×100. Bar graphs show the quantification of Sirius Red–positive area (left) and α-SMA–positive areas (right) in the indicated groups. (**C**) Bar graphs show proliferative response (stimulation index) and cytokine secretion (IFN-γ, TNF-α, IL-2, IL-4, IL-6, IL-10, and IL-17) in splenocytes from untreated (control) and *(Figure legend continues)*

UniFrac distances (40) [q = 0.001, permutational multivariate ANOVA (PERMANOVA) (51), Fig. 9B]. An analysis of composition of microbiomes (52) revealed that this separation may be driven by the differential abundance of several organisms in the J$\alpha18^{-/-}$ mice (Fig. 9C, 9D). Also, α diversity was significantly higher in CD1d$^{-/-}$ mice in comparison with J$\alpha18^{-/-}$ and B6 mice; however, both CD1d$^{-/-}$ and J$\alpha18^{-/-}$ mice showed significant separation in PCoA compared with B6 mice (Supplemental Fig. 3). These results suggest that genetic deficiency of iNKT cells has a strong impact in the microbiota diversity.

When comparing between groups at the phylum level, there were an increased proportion of Proteobacteria and Cyanobacteria in J$\alpha18^{-/-}$ mice as well as Deferribacteres and TM7, which were not detected in B6 mice (Fig. 9C). Similar results were previously reported in the microbiota analysis of CD1$^{-/-}$ mice (53). Only Verrucomicrobia was significantly decreased in J$\alpha18^{-/-}$ mice as compared with B6 mice (Fig. 9C). At the genus level, there was an increased proportion of 17 bacterial genera, including *Bacteroides*, *Lactobacillus*, *Mucispirillum*, and *Prevotella* in J$\alpha18^{-/-}$ mice (Fig. 9D). Interestingly, these four genera have been associated with CD1d$^{-/-}$ mice (53), suggesting that the lack of NKT cells may enable these groups organisms to occupy a greater fraction of the mouse microbiome. β- and δ-proteobacteria have also been reported to be associated with CD1d$^{-/-}$ mice (53), and we observed that the β-proteobacteria genus *Zoogloea* and δ-proteobacteria genera *Desulfovibrio* were present at higher proportion in J$\alpha18^{-/-}$ mice than in B6 mice. Several previously unreported genera were also present at an increased proportion in J$\alpha18^{-/-}$ mice, including Helicobacteraceae family genera, Odoribacter, AF12 (family Rikenellaceae), *Candidatus* Arthromitus (family Clostridiaceae), Parabacteroides and F16 family genera (phylum TM7). In contrast, *Bifidobacterium* that was previously reported to be associated with CD1d$^{-/-}$ mice was present at a decreased proportion in J$\alpha18^{-/-}$ mice (53), suggesting that some of the microbiome effects may be specific to the loss of both type of NKT cells. Others like Clostridiaceae family genera (order Clostridiales), *Coprococcus* and *Ruminococcus* (order Clostridiales, family Lachnospiraceae), *Allobaculum*, and *Akkermansia* were also decreased in J$\alpha18^{-/-}$ mice (Fig. 9D).

In tazarotene-treated B6 mice fed CDAA diet, there was no significant changes to the α diversity compared with B6 mice fed a normal diet or B6 mice fed CDAA diet as measured by Faith PD (Kruskal–Wallis q = 0.88 and q = 0.88, respectively, Fig. 9A). Although a large separation between mice fed a normal diet versus CDAA diet was observed in PCoA space of unweighted UniFrac distances ($q = 0.15 \times 10^{-3}$, PERMANOVA, Fig. 9E), there was a much smaller, although statistically significant, separation between tazarotene-treated and untreated CDAA-fed B6 mice (q = 0.004, PERMANOVA, Fig. 9E). Furthermore, our analysis of composition of microbiomes revealed that the only differences between diets at the phylum level were driven by an increased proportion of Actinobacteria and a decreased proportion of Bacteroidetes in CDAA-fed B6 mice regardless of tazarotene treatment (Fig. 9C). At the genus level, we observed an increased proportion of Desulfovibrio and Clostridiaceae family genera previously reported in CDAA diet–fed mice (54) as well as a significant increase in *Allobaculum*, Erysipelotrichaceae family genera, and Coriobacteriaceae family genera, which were found only in CDAA-fed mice (Fig. 9D). There was a reduction in the proportion of the microbiome represented by Bifidobacterium S24-7 family genera as well as Rikenellaceae family genera, which were previously reported to be decreased in children affected by NASH (55). However, a robust analysis of tazarotene-treated versus untreated CDAA-fed mice was hampered by low number of mice. Together, these results suggest that profound changes in the gut microbiome result from the CDAA diet, but that the differences in composition of the microbiome observed in J$\alpha18^{-/-}$ mice may be driven by events that occur earlier in development rather than as a result of the acute absence of iNKT cells.

Discussion

In this study, we have identified a key innate immune mechanism that is crucial for diet-induced progression from steatosis, steatohepatitis, and fibrosis mediated by differential activation and cytokine secretion by hepatic iNKT cell subsets leading to HSC activation, KCs and CD8$^+$ T cells, and neutrophil infiltration into liver. Thus, in iNKT cell–deficient (J$\alpha18^{-/-}$) mice, as well as in B6 mice following functional inhibition of iNKT cells, hepatic inflammatory infiltration, steatosis, and fibrosis as well as upregulation of key inflammatory genes are significantly blunted. Interestingly, microbial dysbiosis in the absence of iNKT cells may relate to choline-metabolizing bacteria in CDAA diet–fed mice. Importantly, we also found a significant increase in the frequency of CXCR3$^+$/IFN-γ$^+$ iNKT cells in peripheral blood of NASH patients as compared with healthy controls or NAFL patients. Additionally, rapid accumulation of pDC, but not other DC subsets, into liver occurs following feeding of CDAA diet, and genetic depletion of pDC resulted in significant inhibition of the activation of hepatic iNKT cells. Similarly, NASH patients had a significantly high frequency of pDC in PBMCs compared with healthy controls. Collectively, our data indicate a key role for an immune mechanism mediated by the differentially activated hepatic iNKT cell subsets in progression of NASH.

NKT cells have been shown to be either pathogenic or protective in inflammatory liver diseases (9, 17, 56). Some of the discrepancy related to the role of NKT cells in NAFLD may be due to the presence of different subsets of NKT cells as well as the microbial variability in different animal facilities that has a major impact on NKT cells. In this study, we have used two different approaches to demonstrate a pathogenic role of iNKT cells in not only a murine model but also, importantly, their involvement in NASH in humans. First, J$\alpha18^{-/-}$ mice, deficient in iNKT cells but harboring type II NKT cells, are significantly protected from CDAA-induced liver disease (Figs. 2, 3). Secondly, functional inhibition of iNKT cells in tazarotene-treated B6 mice also results in a significant protection from diet-induced hepatic steatosis and fibrosis (Fig. 4). Accordingly, there was similarity in the extent of protection from hepatic damage between tazarotene-treated B6 mice and J$\alpha18^{-/-}$ mice. Contribution from other innate-like cells including MAIT cells cannot be completely ruled out, but based upon the published data from others and our laboratory, it is unlikely that they play any significant role in diet-induced liver disease: 1) CD1d$^{-/-}$ mice, unlike J$\alpha18^{-/-}$ mice (57) that have a full TCRα-chain repertoire and increased number of MAIT cells (58, 59), are similarly significantly

tazarotene-treated mice (n = 5 mice per group) in response to an in vitro challenge with αGalCer at an optimum concentration (1 ng/ml). (**D**) Bar graph shows the percentage of αGalCer/CD1d tetramer$^+$ TCRβ$^+$ cells in liver of CDAA-fed B6 mice untreated or treated with tazarotene (top panel). Representative gel of Vα14Jα18 mRNA expression in liver from untreated and tazarotene-treated mice (bottom panel). All data are presented as mean ± SEM. Data representative of three independent experiments. *$p < 0.05$, **$p \leq 0.01$, ***$p \leq 0.001$, ****$p \leq 0.0001$ by unpaired t test. n.d., not detected; Untd, untreated; Taz., tazarotene.

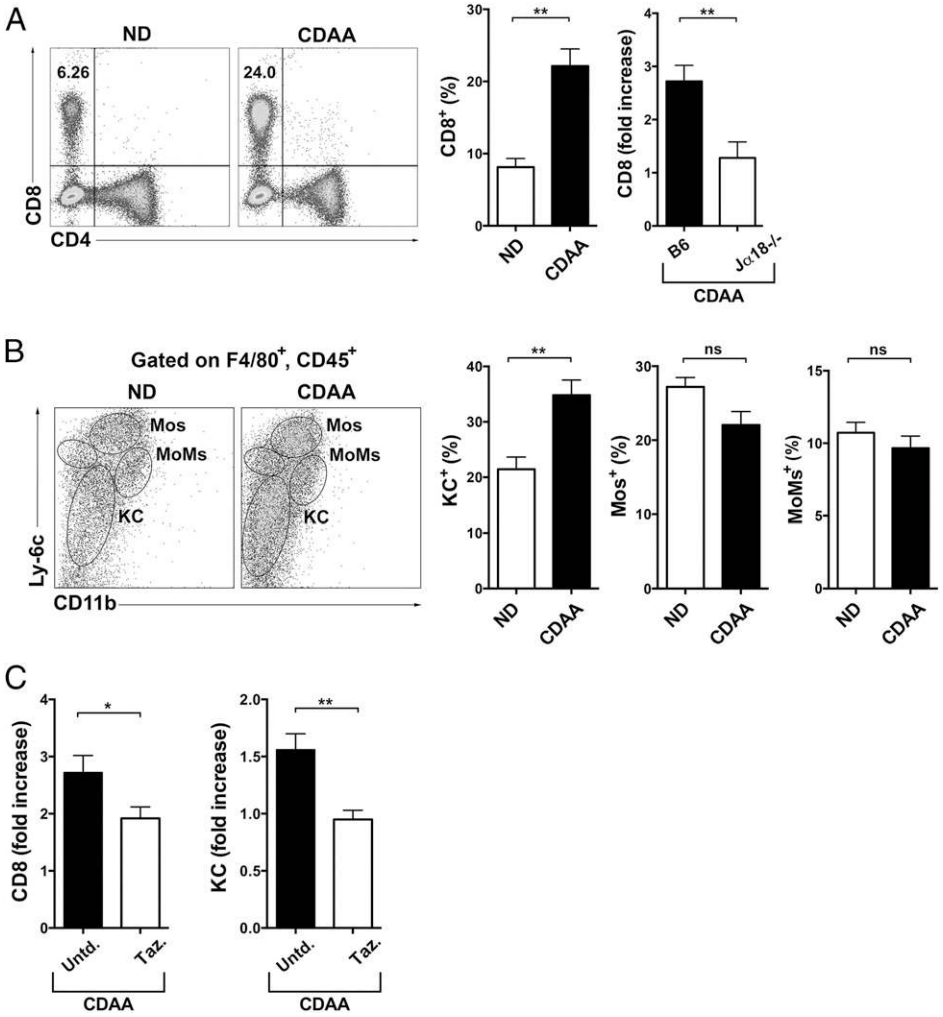

FIGURE 5. Hepatic infiltration by $CD8^+$ T cells and macrophages following CDAA diet is dependent on iNKT cells. B6 and $J\alpha18^{-/-}$ mice were fed normal diet (ND) or CDAA diet for 20 wk. (**A**) Representative dot plot of $CD8^+$ T cells in liver of B6 mice fed ND or CDAA diet. Numbers on dot plots indicate percentage of $CD8^+$ T cells on the lymphocyte gate. Bar graphs show the percentage of $CD8^+$ T cells (left) in liver of B6 mice after 20 wk of ND or CDAA diet and fold increase of $CD8^+$ T cells (right) in liver of B6 and $J\alpha18^{-/-}$ mice fed CDAA diet. Fold increase was obtaining by dividing the percentages of $CD8^+$ T cells in liver of B6 or $J\alpha18^{-/-}$ mice fed CDAA diet by that in liver of ND-fed B6 mice. At least four mice per group. (**B**) Representative dot plots of liver macrophages cells in B6 mice fed ND or CDAA diet. Gated on $CD45^+F4/80^+$ cells, KCs were defined as Ly-$6C^{lo}CD11b^{lo}$, inflammatory Mos as Ly-$6C^{hi}CD11b^{int}$, and Mo-derived macrophages (MoMs) as Ly-$6C^{int}CD11b^{hi}$, as described before (32). Each subset is indicated on the dot plots. Bar graphs show the percentage of KCs, Mos, and MoMs in liver of B6 mice fed ND ($n = 4$) or CDAA ($n = 7$–9) diet. (**C**) Bar graphs show the fold increase of $CD8^+$ T cells (left) and KCs (right) in liver of CDAA-fed B6 mice untreated or treated with tazarotene. Fold increase was obtaining by dividing the percentage of $CD8^+$ T cells or KCs in liver of untreated or tazarotene-treated CDAA-fed B6 mice by that in liver of ND-fed B6 mice. B6 mice maintained on CDAA diet for 20 wk were subjected to i.p. injection of tazarotene (300 μg/mouse) twice per week or left untreated. All data are presented as mean ± SEM. Data representative of three independent experiments. $^*p < 0.05$, $^{**}p \leq 0.01$ by unpaired two-sample t test. Untd, untreated; Taz, tazarotene.

protected from diet-induced hepatic steatosis and fibrosis (26, 47, 60); 2) anti-CD1d Ab treatment also inhibits diet-induced hepatic disease (19); 3) there is a significant increase in the number of hepatic pDC in the murine model as well as in NASH patients and their important role in activation of iNKT cells; and 4) there is a significant increase in activated proinflammatory iNKT cells in NASH patients in comparison with NAFL patients and healthy subjects. Collectively, our data in murine models and in NASH patients indicate that iNKT cells play an important role in inflammatory liver diseases.

Although, a reduction in iNKT cell numbers has been reported following methionine/choline-deficient or high-fat diets (HFD) as well as in obese ob/ob mice and KK-A(y) diabetic mice (29, 61–65), none of these models have evaluated TCR or NK1.1 downmodulation, specifically on $tetramer^+$ cells. Interestingly, in some cases, proinflammatory activated KC have been shown to induce apoptosis of overactivated iNKT cells following HFD (66). We found that the number of αGalCer/CD1d-$tetramer^+$ cells is progressively reduced in liver of B6 mice following CDAA diet and that the majority of $tetramer^+$ cells had reduced surface expression of NK1.1. However, the intrahepatic mRNA level of the invariant Vα14-Jα18 TCR expressed by iNKT cells did not decrease, but rather increased following CDAA diet (Fig. 1). These results suggest that long-term feeding of CDAA diet leads to chronic iNKT cells activation and downmodulation of their surface expression of TCR and NK1.1. It is known that after stimulation with αGalCer or IL-12, iNKT cells can become undetectable because of downmodulation of surface TCR and NK1.1 expression (67–69). Furthermore, progressively increased proinflammatory cytokine secretion by iNKT cells following CDAA diet further indicates their chronic activation.

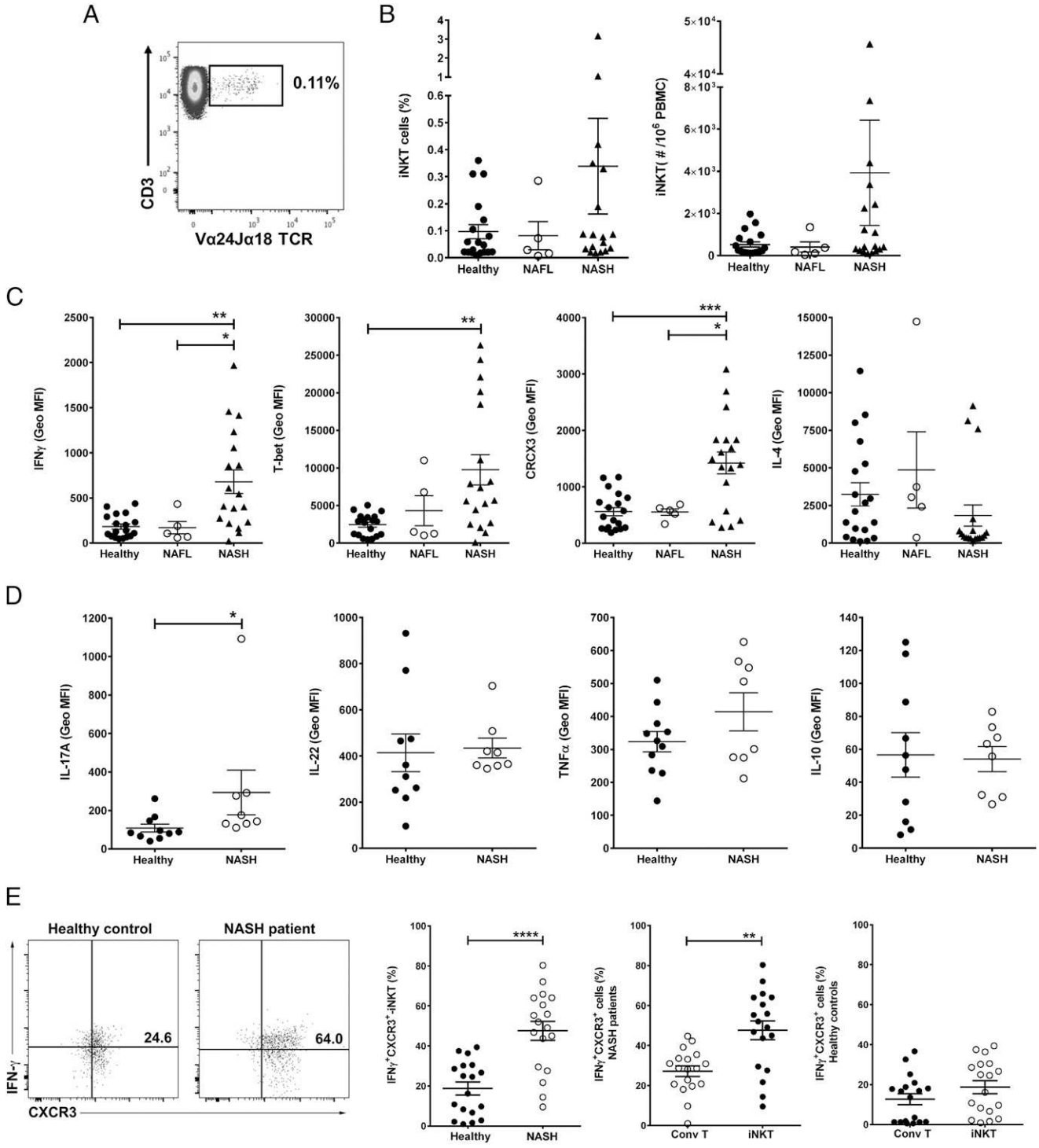

FIGURE 6. iNKT cells from NASH patients are activated and secrete proinflammatory cytokines. PBMC were analyzed by multiparameter flow cytometry. iNKT cells were identified using the following gate strategy: first, lymphocytes were gated based on forward light scatter (FSC) and side light scatter (SSC), and singlet live cells were selected. $CD19^+$ cells were excluded, and $CD3^+$ T cells were gated in the $CD19^-$ gate. iNKT cells were defined as double CD3- and Vα24-Jα18 TCR–positive cells ($CD3^+V\alpha24J\alpha18TCR^+$) in the $CD3^+$ gate and were expressed as percentage of $CD3^+$ T cells. Conventional T cells were identified as CD3-positive and simultaneously as Vα24-Jα18 TCR–negative cells ($CD3^+/V\alpha24\text{-}J\alpha18\ TCR^-$) in the live/$CD19^-$ gate. (**A**) Representative dot plot of iNKT cells in PBMC from healthy control. Number on dot plot indicate the percentage of iNKT cells within the drawn gate. (**B**) Scatter graphs show the cumulative results of the percentage (left) and numbers (right) of iNKT cells in PBMC from healthy controls (n = 19) and patients with NAFL (n = 5) or NASH (n = 18). (**C**) Scatter graphs show the geometric MFI of IFN-γ, T-bet, CXCR3, and IL-4 staining of unstimulated iNKT cells in PBMC from healthy controls and patients with NAFL or NASH. (**D**) Scatter graphs show the geometric MFI of IL-17A, IL-22, TNF-α, and IL-10 staining of unstimulated iNKT cells in PBMC of NASH patients (n = 8) and healthy controls (n = 10–11). (**E**) Representative dot plots of IFN-γ^+CXCR3^+ double-positive cells in the iNKT gate in PBMC of healthy controls and NASH patients. Scatter graphs show the percentage of IFN-γ^+CXCR3^+ iNKT cells in PBMC of healthy controls (n = 18) and NASH patients (n = 18) (left) and the percentage of IFN-γ^+CXCR3^+ double-positive cells in the conventional $CD3^+$ T cell gate (Conv T) and iNKT gate in PBMC of NASH patients (center) and healthy control (right). Conv T were identified as $CD3^+V\alpha24J\alpha18TCR^-$ cells in the $CD3^+$ gate. Each point represents an individual. All data are presented as mean ± SEM. $^*p \le 0.05$, $^{**}p \le 0.01$, $^{***}p \le 0.001$, $^{****}p \le 0.0001$ by one-way ANOVA or Mann–Whitney U test.

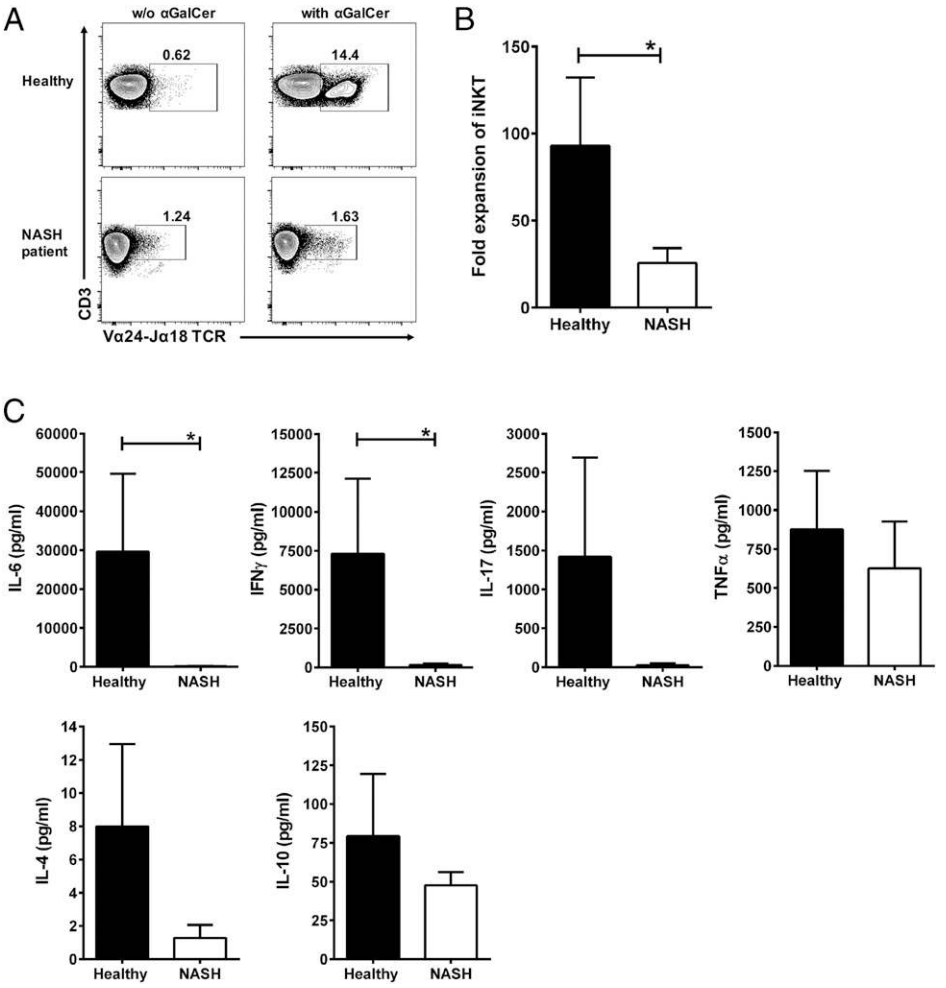

FIGURE 7. iNKT cells in NASH patients are hyporesponsive to an in vitro stimulation with αGalCer. Fresh PBMCs from NASH patients ($n = 8$) and healthy controls ($n = 9$) were cultured (2×10^6/well) in duplicate for 10 d with αGalCer (100 ng/ml) in 200 μl of completed RPMI medium plus 40 U/ml human rIL-2 in flat-bottom 96-well plates at 37°C in an atmosphere containing 5% CO_2. Supernatants collected after 4 d of culture. (**A**) Representative contour plots of iNKT cells in PBMC of healthy controls (top) and NASH patients (bottom) after 10-d culture without or with αGalCer. Numbers on dot plots indicate the percentage of iNKT cells. (**B**) Bar graph show the fold expansion of iNKT cells in PBMC of healthy controls and NASH patients after 10-d culture with αGalCer. The fold expansion of iNKT cells was obtained by dividing the percentage of iNKT cells after 10-d culture by that on day 0 (fresh PBMC). (**C**) Bar graphs show the quantification of IL-6, IFN-γ, IL-17, TNF-α, IL-4, and IL-10 (picograms per milliliter) in culture supernatants from PBMC of healthy controls and NASH patients after 4-d culture with αGalCer. Cytokine secretion was quantified using BD Cytometric Bead Array (CBA) Human Th1/Th2/Th17 Cytokine Kit. All data are presented as mean ± SEM. $*p \leq 0.05$ by Mann–Whitney U test.

Another important finding in our study is that IL-17$^+$– and IL-22$^+$–iNKT cells (NKT17) are dominant early during liver steatosis, whereas IFN-γ$^+$ and IL-4$^+$ or IL-13$^+$ (NKT1/NKT2) cells prevail later during fibrosis following CDAA diet (Fig. 1). Notably, activated IFN-γ– and IL-17A–secreting iNKT cells are also present in high frequency in peripheral blood of NASH patients (Fig. 6) in comparison with those in NAFL patients or healthy controls. Additionally, NASH patients with advanced liver fibrosis had low levels of IL-17A and high levels of IFN-γ compared with patients with less fibrosis (data not shown). Although an important pathogenic role for IFN-γ– (Th1) and IL-17– (Th17) secreting conventional CD4$^+$ T cells in the progression of NAFLD in both mice and humans has been suggested (70, 71), our study indicates that early cytokine secretion by iNKT cells may set the stage for changes in conventional CD4$^+$ T cells during NASH progression. Consistent with our data, IL-17 signaling has been shown to stimulate liver inflammatory cells, like KCs and macrophages, to produce proinflammatory cytokines, IL-1, IL-6, and TNF-α as well as the fibrogenic cytokine, TGF-β. IL-17 also induces activation of HSC to produce collagen type I, thus, promoting their differentiation into fibrogenic myofibroblasts via Stat3 signaling pathway (71–75). Consistently, high IL-17 levels as well as high hepatic expression of Th17 cell–related genes have been associated with hepatic steatosis in patients with NASH (76, 77). Thus, our data suggest that different iNKT cell subsets participate in the progression from steatosis to steatohepatitis and fibrosis in NASH.

Our study also suggests an important role of iNKT cells in HSC activation that mediates hepatic fibrosis following CDAA diet. Thus, CDAA feeding of B6 mice led to increased frequency of IL-13$^+$ iNKT cells accompanied by HSC activation as shown by an increase in α-SMA–positive cells. Furthermore, α-SMA staining as well as expression of genes indicative of fibrosis, including α-SMA, TIMP-1, COL1, and CTGF, was significantly reduced in liver of CDAA-fed Jα18$^{-/-}$ mice. Consistent with our data, methionine/choline-deficient diet also resulted in hepatic iNKT cell stimulation of HSC activation and fibrosis through production of hedgehog protein and osteopontin (26). Similarly, IL-13 secretion by iNKT cells can also promote HSC activation. Accordingly, a profibrotic role for TGF-β/Smad signaling and IL-13 in activation of HSC as well as in upregulation of collagen I and fibrosis-associated genes, like α-SMA and CTGF, in HSC has been shown (78, 79). Furthermore, high serum levels of IL-13 as well as upregulation of IL-13 and IL-13Rα2 expression have been found in activated HSC in liver biopsies from NASH patients (80).

Our data showed that CDAA diet induced a significant increase in liver infiltrating CD8$^+$ T cells and KCs (Fig. 5) that is dependent on iNKT cells because it is reduced significantly in either Jα18$^{-/-}$ mice or following functional inhibition of iNKT cell in B6 mice. We propose that the activation of IFN-γ–secreting iNKT cells results in cross-priming of conventional CD8$^+$ T cells that have been shown to be pathogenic in liver disease following high-fat, high-fat high-cholesterol, or choline-deficient high-fat diets (28, 47, 81, 82). Consistent with the potential pathogenic role of CD8$^+$ T cells in liver, increased numbers of infiltrating CD8$^+$ T cells have been found in livers from NASH patients (28, 47, 81).

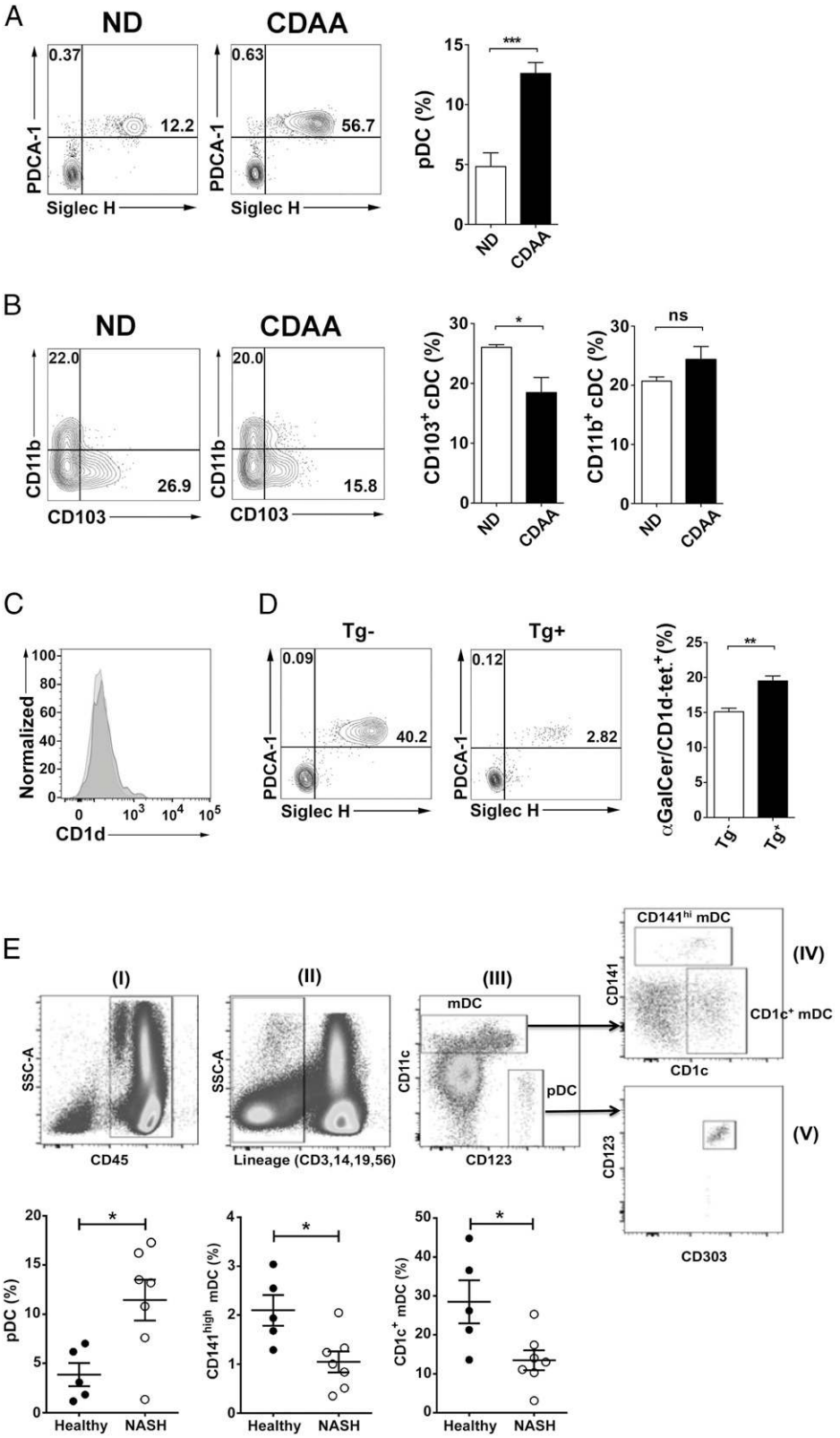

FIGURE 8. DC subsets are altered and are involved in iNKT activation in both murine and human NASH. (**A**) Representative contour plots of pDC in liver of B6 mice fed normal diet (ND) or CDAA diet. pDCs were identified as double PDCA-1– and Siglec H–positive cells (PDCA-1$^+$Siglec H$^+$) in the live$^+$CD3$^-$CD45$^+$CD11c$^+$CD11b$^-$B220$^+$ gate. Numbers on plots indicate the percentage of pDC. Bar graph shows the percentage of pDC in B6 mice fed ND (n = 8) or CDAA diet (n = 6). (**B**) Representative contour plots of the two major cDC subsets, CD103$^+$ cDC and CD11b$^+$ cDC, in liver of B6 mice fed ND or CDAA diet. The CD103$^+$ cDC subset was identified as CD103-positive and simultaneously CD11b-negative cells (CD103$^+$/CD11b$^-$) in the live$^+$CD3$^-$CD19$^-$CD45$^+$MHC-II$^+$CD11c^{hi} gate. The CD11b$^+$ cDC subset was identified as CD11b-positive and simultaneously CD103-negative cells (CD11b$^+$/CD103$^-$) in the live$^+$CD3$^-$CD19$^-$CD45$^+$MHC-II$^+$CD11c^{hi} gate. Numbers on plots indicate the percentage of both subsets. Bar graphs show the percentage of CD103$^+$ cDC (left) and CD11b$^+$ cDC (right) in the indicated groups. Each group included three mice. (**C**) Histogram shows representative CD1d expression on gated pDCs in liver of B6 mice fed ND or CDAA diet. (**D**) Representative contour plots of pDCs in liver of *(Figure legend continues)*

Our data in human PBMC indicate that $CD8^+$ T cells are not significantly increased in peripheral blood of NASH patients compared with healthy controls and is consistent with the hypothesis that $CD8^+$ T cells may have migrated into liver (28, 83). It has been shown that KCs also play a key proinflammatory role in liver damage in NASH via inflammatory cytokines, such as TNF-α, IL-1β, and reactive oxygen species. Thus, depletion of KCs by i.v. injection of liposomal clodronate results in improvement of hepatic steatosis, inflammatory cell infiltration, and metabolic disease (84–87). Collectively, these results indicated that diet-induced HSC activation and hepatic infiltration by $CD8^+$ T and KCs is dependent on the presence of activated iNKT cells, suggesting that iNKT cells in collaboration with $CD8^+$ T cells and KCs are drivers in the pathogenesis of NASH.

Earlier studies related to the analysis of NKT cells in human NAFLD have caveats because of the use of nonspecific markers like $CD3^+CD56^+$ to identify iNKT cells. In our study, to differentiate iNKT cells from other T cells, including type II NKT cells, we have used a clonotypic mAb Vα24Jα18 TCR, which specifically identifies iNKT cells. Our data indicated that NASH patients have a significantly higher frequency of activated proinflammatory IFN-γ– and IL-17–secreting iNKT cells in peripheral blood (Fig. 6) in comparison with those from NAFL patients or healthy controls, suggesting their important role in the progression from NAFL to NASH. Consistent with our findings, it has been reported that $CD3^+CD56^+$ NKT–like cells are increased in liver and peripheral blood of NAFLD patients with moderate to severe steatosis (88–90). In addition, Tajiri et al. (91) reported that $CD3^+CD56^+V\alpha24^+$ iNKT cells were increased in both liver and peripheral blood of NAFLD patients as the disease activity increased. Consistent with our data, lower frequency of peripheral $CD3^+CD56^+V\alpha24^+$ iNKT cells was found in patients with only steatosis and no steatohepatitis (92). Additionally, our data suggest that iNKT cells are chronically activated in vivo in NASH patients as indicated by their hyporesponsiveness to ex vivo stimulation with αGalCer (Fig. 7). Similar ex vivo hyporesponsiveness has been shown in other clinical conditions in which iNKT cells are chronically stimulated, including autoimmune disease and cancer patients (93, 94). Collectively, these data suggest a potentially important role of iNKT cells for progression from NAFL to NASH in humans. Additionally, a subset of IFN-γ^+CXCR3^+ iNKT cells is highly represented in NASH patients, suggesting that this could constitute a novel immunological marker for NASH progression.

Our study also indicates a rapid accumulation of pDC, but not other DC subsets in liver of B6 mice, following CDAA diet (Fig. 8). Furthermore, selective depletion of pDC in vivo using BDCA2-DTR mice (95) leads to a significant inhibition of hepatic iNKT TCR downmodulation, suggesting pDC involvement in iNKT cell activation. Because complete depletion of pDC in these mice after DT administration is only sustained for short time (96), we were unable to investigate pDC depletion effect on NASH progression. Consistently, pDC accumulation in liver and adipose tissue has been recently shown in HFD-induced inflammation (97). We propose that damage of hepatocytes in CDAA-fed mice induces the release of mitochondrial DNA (mtDNA), a TLR9 ligand. Because pDC are the major early responders of TLR9, we speculate that mtDNA released from injured hepatocytes leads to accumulation of pDC in liver, followed by iNKT activation in a TLR9-dependent manner (15, 98). Recently, hepatic mitochondrial damage has also been reported in NASH patients (99, 100) and increased plasma levels of mtDNA in both HFD-induced murine model as well as in NASH patients have been shown to trigger TLR9 pathway to induce steatosis (101, 102). Notably, rapid accumulation of pDC in the pancreas has been shown to initiate autoimmune diabetes in NOD mice (103). At present, we cannot rule out the importance of other cDC subsets in activation of iNKT cells in our model. It is possible that following chronic feeding of CDAA diet, altered gut microbiota could provide the necessary milieu in the gut to facilitate migration of $CD103^+$ cDC into liver, where they can cross-prime IFN-γ^+-iNKT cells and conventional $CD8^+$ T cells (104, 105), (S. Dasgupta, unpublished observations). A $CD103^+$ DC resembling lymphoid tissue–resident $CD8^+$ cDC has recently been shown to be the major APCs in iNKT cell activation (97, 106). Consistent with this hypothesis, our preliminary data using Kaede mice suggest that there is a migration of $CD103^+CD11b^-$ cells, but not $CD11b^+$ DC, from the major lymph nodes, draining both small and large intestines into liver in the noninflamed steady state (S. Dasgupta, unpublished observations). Accordingly, following chronic feeding (4–5 mo), $CD11b^+$ cDC and $CD103^+$ cDC are increased in liver (S. Dasgupta, unpublished observations). A cross-talk between pDC and cDC has been shown to be crucial in the priming of $CD8^+$ T cells in the antitumor immunity (107, 108). Our results showing increased frequency of pDC in peripheral blood of NASH patients (Fig. 8) are in agreement with published data that show positive correlation between diseased livers and increased frequency of $CD123^+$ pDC and decreased frequency of $CD141^+$ mDC (109).

The role that the gut microbiome may play in the development of disease in the CDAA diet–fed mouse model of NASH remains unclear. It is evident that the introduction of the CDAA diet causes a profound shift in the composition of the gut microbiome (Fig. 9), and the inhibition of iNKT cells largely does not restore the composition to reflect a normal diet nor the $J\alpha18^{-/-}$ mouse composition. As the overall diversity of the gut microbiome in B6 mice is not altered by the CDAA diet, an imbalance or dysbiotic state driven by the large changes in nutrient availability may be a driver in the development of CDAA diet–induced NASH. Intriguingly, many of the genera that appeared to be increased in CDAA-fed mice were identified to be associated with choline consumption and the increased production of trimethylamine, which is converted to the obesogenic compound trimethylamine-N-oxide in the liver (110). Because 16S rRNA sequencing data are compositional, it is not possible to say if the total amount of bacteria in each of these

BDCA2-DTR transgenic (Tg^+) and littermate (Tg^-) mice on CDAA diet after DT administration. Bar graph shows the percentage of iNKT cells (αGalCer/CD1d tetramer$^+$) in liver of Tg^- ($n = 3$) and Tg^+ ($n = 3$) mice after DT treatment. All data presented in (A), (B), and (D) are presented as mean ± SEM and are representative of three independent experiments. $*p \leq 0.05$, $**p \leq 0.01$, $***p \leq 0.001$ by unpaired two-sample t test. (**E**) Representative dot plots of gating strategy to identify DC subsets in human PBMC. DCs were gated based on forward light scatter (FSC) and side light scatter (SSC), including both lymphocytes and Mos. Doublets and dead cells were excluded. (Graph I) $CD45^+$ cells were selected on gated live singlet cells. (Graph II) Lineage (CD3/19/56/14)–negative cells were gated on $CD45^+$ cells. (Graph III) Based on CD11c and CD123 expression, pDC were identified as $CD123^+CD11c^-$ cells, whereas mDC were identified as $CD11c^+CD123^-$ cells. (Graph IV) Based on CD141 and CD1c expression, mDCs were divided in $CD141^{hi}$ cells or $CD1c^+$ cells. (Graph V) The pDC lineage was confirmed by expression of CD303. Scatter graphs show the percentage of pDC (left), $CD141^{hi}$ mDC (center), and $CD1c^+$ mDC (right) in PBMC of healthy controls ($n = 5$) and NASH patients ($n = 7$). Each point represents an individual. All data are presented as mean ± SEM. $*p \leq 0.05$ by Mann–Whitney U test.

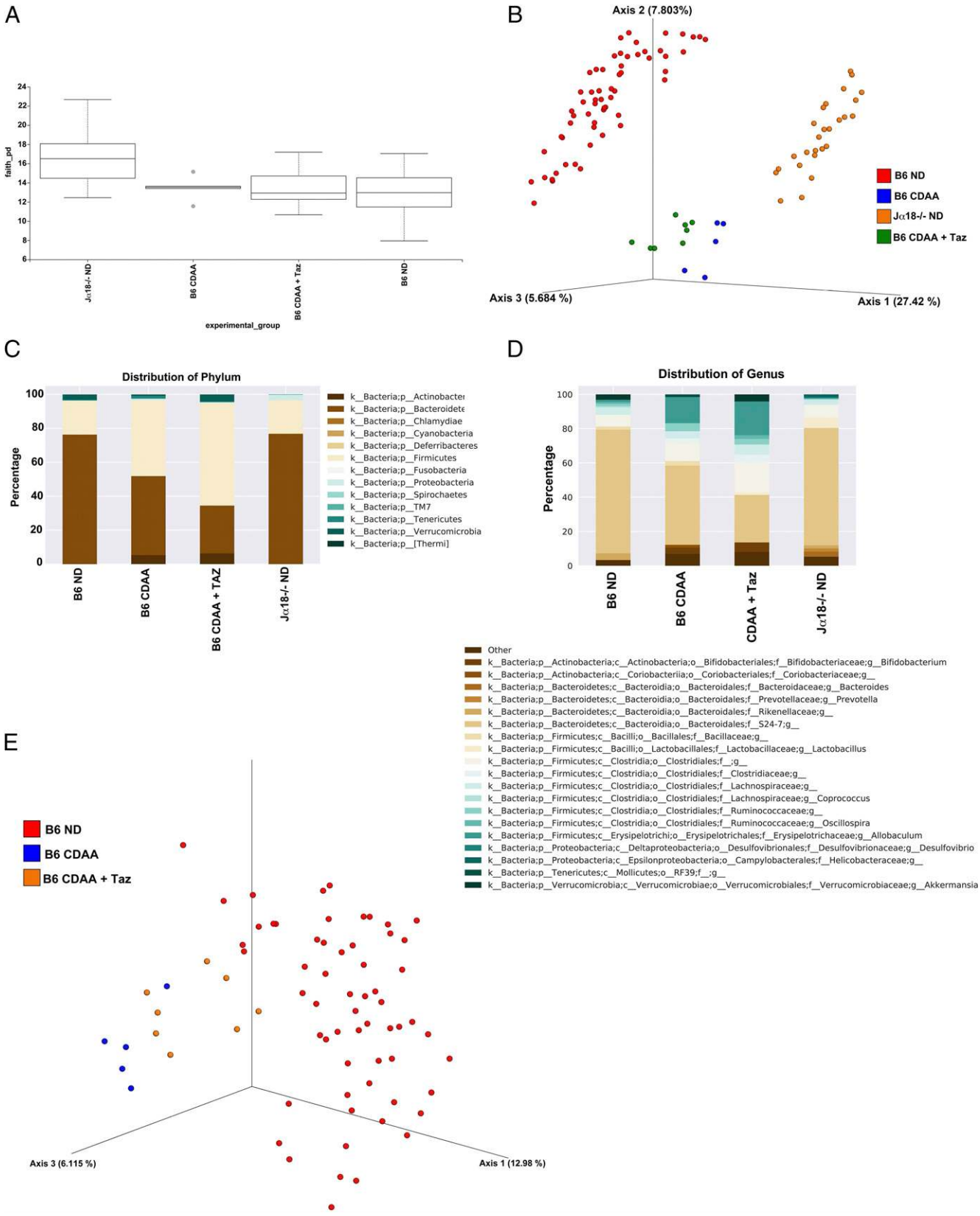

FIGURE 9. Differential microbial diversity in mice lacking functional iNKT cells. J$\alpha18^{-/-}$ (n = 26) and B6 (n = 60) mice were maintained on normal diet (ND). B6 mice maintained on CDAA diet for 20 wk were subjected to i.p. injection of tazarotene (300 μg/mouse) twice per week (n = 8) or left untreated (n = 5). All groups were housed in separate cages. Genomic bacterial DNA was isolated from fecal samples and the V4 region of 16S rDNA was amplified and sequenced. (**A**) Box-plot of Faith α PD for each of the experimental groups; bars indicate the interquartile range. (**B**) Discrimination of mice groups based on PCoA of UniFrac distance. Red, B6, ND; blue, B6, CDAA diet; green, B6, CDAA^{+}Taz; Orange, J$\alpha18^{-/-}$, ND. (**C**) Summary of the average representation of bacterial phyla detected in these samples. (**D**) Summary of the average representation of bacterial genera detected in these samples. (**E**) PCoA of J$\alpha18^{-/-}$ versus B6 mice with and without CDAA diet and tazarotene treatment. Red, B6, ND; blue, B6, CDAA diet; orange, B6, CDAA^{+}Taz.

groups is increased or if others are proportionately decreased, but rather only that a shift is evident in the community as a result of an altered equilibrium (52, 111). Likewise, the lack of evidence for a given organism or group of organisms does not conclusively rule out their presence because experimental and bioinformatics techniques can provide false negatives, but does indicate an underrepresentation of the organism in the selection of sequences analyzed in this current study that may be driven by biologic effects. As this is, to our knowledge, the first report of the gut microbiome composition in J$\alpha 18^{-/-}$ mice, many follow-up experiments to examine the strain-level associations and related changes to the host and gut metabolome are warranted. We are also investigating whether alterations in self- or microbial lipids are involved in activation of iNKT cells.

Collectively, our data not only show an important role of iNKT cell subset activation in diet-induced progression from steatosis to fibrosis, but also a notable similarity with human NAFLD showing a significant increase in activation of iNKT cells in peripheral blood of NASH patients.

Acknowledgments

This work was performed with the support of the Flow Cytometry Core at the Veterans Affairs San Diego Health Care System and the San Diego Veterans Medical Research Foundation. We thank Gregory Humphrey, Cole Heale, and Tara Schwartz for sample processing and Gail Ackermann for assistance with metadata curation and data handling.

Disclosures

V.K. is a scientific cofounder of and a consultant for GRI-Bio, La Jolla, CA. The other authors have no financial conflicts of interest.

References

1. Wree, A., L. Broderick, A. Canbay, H. M. Hoffman, and A. E. Feldstein. 2013. From NAFLD to NASH to cirrhosis-new insights into disease mechanisms. *Nat. Rev. Gastroenterol. Hepatol.* 10: 627–636.
2. Heymann, F., and F. Tacke. 2016. Immunology in the liver--from homeostasis to disease. *Nat. Rev. Gastroenterol. Hepatol.* 13: 88–110.
3. Greuter, T., H. Malhi, G. J. Gores, and V. H. Shah. 2017. Therapeutic opportunities for alcoholic steatohepatitis and nonalcoholic steatohepatitis: exploiting similarities and differences in pathogenesis. *JCI Insight* 2: e95354.
4. Anstee, Q. M., and C. P. Day. 2013. The genetics of NAFLD. *Nat. Rev. Gastroenterol. Hepatol.* 10: 645–655.
5. Brennan, P. J., M. Brigl, and M. B. Brenner. 2013. Invariant natural killer T cells: an innate activation scheme linked to diverse effector functions. *Nat. Rev. Immunol.* 13: 101–117.
6. Godfrey, D. I., and M. Kronenberg. 2004. Going both ways: immune regulation via CD1d-dependent NKT cells. *J. Clin. Invest.* 114: 1379–1388.
7. Godfrey, D. I., A. P. Uldrich, J. McCluskey, J. Rossjohn, and D. B. Moody. 2015. The burgeoning family of unconventional T cells. *Nat. Immunol.* 16: 1114–1123.
8. Kumar, V. 2013. NKT-cell subsets: promoters and protectors in inflammatory liver disease. *J. Hepatol.* 59: 618–620.
9. Marrero, I., R. Ware, and V. Kumar. 2015. Type II NKT cells in inflammation, autoimmunity, microbial immunity, and cancer. *Front. Immunol.* 6: 316.
10. Exley, M., J. Garcia, S. P. Balk, and S. Porcelli. 1997. Requirements for CD1d recognition by human invariant Valpha24+ CD4-CD8- T cells. *J. Exp. Med.* 186: 109–120.
11. Exley, M. A., N. J. Bigley, O. Cheng, A. Shaulov, S. M. Tahir, Q. L. Carter, J. Garcia, C. Wang, K. Patten, H. F. Stills, et al. 2003. Innate immune response to encephalomyocarditis virus infection mediated by CD1d. *Immunology* 110: 519–526.
12. Girardi, E., I. Maricic, J. Wang, T. T. Mac, P. Iyer, V. Kumar, and D. M. Zajonc. 2012. Type II natural killer T cells use features of both innate-like and conventional T cells to recognize sulfatide self antigens. *Nat. Immunol.* 13: 851–856.
13. Arrenberg, P., R. Halder, Y. Dai, I. Maricic, and V. Kumar. 2010. Oligoclonality and innate-like features in the TCR repertoire of type II NKT cells reactive to a beta-linked self-glycolipid. *Proc. Natl. Acad. Sci. USA* 107: 10984–10989.
14. Jahng, A., I. Maricic, C. Aguilera, S. Cardell, R. C. Halder, and V. Kumar. 2004. Prevention of autoimmunity by targeting a distinct, noninvariant CD1d-reactive T cell population reactive to sulfatide. *J. Exp. Med.* 199: 947–957.
15. Montoya, C. J., H. B. Jie, L. Al-Harthi, C. Mulder, P. J. Patiño, M. T. Rugeles, A. M. Krieg, A. L. Landay, and S. B. Wilson. 2006. Activation of plasmacytoid dendritic cells with TLR9 agonists initiates invariant NKT cell-mediated cross-talk with myeloid dendritic cells. *J. Immunol.* 177: 1028–1039.
16. Arrenberg, P., I. Maricic, and V. Kumar. 2011. Sulfatide-mediated activation of type II natural killer T cells prevents hepatic ischemic reperfusion injury in mice. *Gastroenterology* 140: 646–655.
17. Halder, R. C., C. Aguilera, I. Maricic, and V. Kumar. 2007. Type II NKT cell-mediated anergy induction in type I NKT cells prevents inflammatory liver disease. *J. Clin. Invest.* 117: 2302–2312.
18. Maricic, I., H. Sheng, I. Marrero, E. Seki, T. Kisseleva, S. Chaturvedi, N. Molle, S. A. Mathews, B. Gao, and V. Kumar. 2015. Inhibition of type I natural killer T cells by retinoids or following sulfatide-mediated activation of type II natural killer T cells attenuates alcoholic liver disease in mice. *Hepatology* 61: 1357–1369.
19. Mathews, S., D. Feng, I. Maricic, C. Ju, V. Kumar, and B. Gao. 2016. Invariant natural killer T cells contribute to chronic-plus-binge ethanol-mediated liver injury by promoting hepatic neutrophil infiltration. *Cell. Mol. Immunol.* 13: 206–216.
20. Eguchi, A., X. De Mollerat Du Jeu, C. D. Johnson, A. Nektaria, and A. E. Feldstein. 2016. Liver Bid suppression for treatment of fibrosis associated with non-alcoholic steatohepatitis. *J. Hepatol.* 64: 699–707.
21. Kodama, Y., T. Kisseleva, K. Iwaisako, K. Miura, K. Taura, S. De Minicis, C. H. Osterreicher, B. Schnabl, E. Seki, and D. A. Brenner. 2009. c-Jun N-terminal kinase-1 from hematopoietic cells mediates progression from hepatic steatosis to steatohepatitis and fibrosis in mice. *Gastroenterology* 137: 1467–1477.e5.
22. Nakae, D., H. Yoshiji, Y. Mizumoto, K. Horiguchi, K. Shiraiwa, K. Tamura, A. Denda, and Y. Konishi. 1992. High incidence of hepatocellular carcinomas induced by a choline deficient L-amino acid defined diet in rats. *Cancer Res.* 52: 5042–5045.
23. Corbin, K. D., and S. H. Zeisel. 2012. Choline metabolism provides novel insights into nonalcoholic fatty liver disease and its progression. *Curr. Opin. Gastroenterol.* 28: 159–165.
24. Guerrerio, A. L., R. M. Colvin, A. K. Schwartz, J. P. Molleston, K. F. Murray, A. Diehl, P. Mohan, J. B. Schwimmer, J. E. Lavine, M. S. Torbenson, and A. O. Scheimann. 2012. Choline intake in a large cohort of patients with nonalcoholic fatty liver disease. *Am. J. Clin. Nutr.* 95: 892–900.
25. Zeisel, S. H. 2010. Choline: clinical nutrigenetic/nutrigenomic approaches for identification of functions and dietary requirements. *World Rev. Nutr. Diet.* 101: 73–83.
26. Syn, W. K., K. M. Agboola, M. Swiderska, G. A. Michelotti, E. Liaskou, H. Pang, G. Xie, G. Philips, I. S. Chan, G. F. Karaca, et al. 2012. NKT-associated hedgehog and osteopontin drive fibrogenesis in non-alcoholic fatty liver disease. *Gut* 61: 1323–1329.
27. Hebbard, L., and J. George. 2011. Animal models of nonalcoholic fatty liver disease. *Nat. Rev. Gastroenterol. Hepatol.* 8: 35–44.
28. Wolf, M. J., A. Adili, K. Piotrowitz, Z. Abdullah, Y. Boege, K. Stemmer, M. Ringelhan, N. Simonavicius, M. Egger, D. Wohlleber, et al. 2014. Metabolic activation of intrahepatic CD8+ T cells and NKT cells causes nonalcoholic steatohepatitis and liver cancer via cross-talk with hepatocytes. *Cancer Cell* 26: 549–564.
29. Li, Z., M. J. Soloski, and A. M. Diehl. 2005. Dietary factors alter hepatic innate immune system in mice with nonalcoholic fatty liver disease. *Hepatology* 42: 880–885.
30. Kawano, T., J. Cui, Y. Koezuka, I. Toura, Y. Kaneko, K. Motoki, H. Ueno, R. Nakagawa, H. Sato, E. Kondo, et al. 1997. CD1d-restricted and TCR-mediated activation of valpha14 NKT cells by glycosylceramides. *Science* 278: 1626–1629.
31. Mendiratta, S. K., W. D. Martin, S. Hong, A. Boesteanu, S. Joyce, and L. Van Kaer. 1997. CD1d1 mutant mice are deficient in natural T cells that promptly produce IL-4. *Immunity* 6: 469–477.
32. Thompson, L. R., J. G. Sanders, D. McDonald, A. Amir, J. Ladau, K. J. Locey, R. J. Prill, A. Tripathi, S. M. Gibbons, G. Ackermann, et al; Earth Microbiome Project Consortium. 2017. A communal catalogue reveals Earth's multiscale microbial diversity. *Nature* 551: 457–463.
33. Walters, W., E. R. Hyde, D. Berg-Lyons, G. Ackermann, G. Humphrey, A. Parada, J. A. Gilbert, J. K. Jansson, J. G. Caporaso, J. A. Fuhrman, et al. 2015. Improved bacterial 16S rRNA gene (V4 and V4-5) and fungal internal transcribed spacer marker gene primers for microbial community surveys. *mSystems* 1: e00009-15.
34. Caporaso, J. G., J. Kuczynski, J. Stombaugh, K. Bittinger, F. D. Bushman, E. K. Costello, N. Fierer, A. G. Peña, J. K. Goodrich, J. I. Gordon, et al. 2010. QIIME allows analysis of high-throughput community sequencing data. *Nat. Methods* 7: 335–336.
35. Bokulich, N. A., S. Subramanian, J. J. Faith, D. Gevers, J. I. Gordon, R. Knight, D. A. Mills, and J. G. Caporaso. 2013. Quality-filtering vastly improves diversity estimates from Illumina amplicon sequencing. *Nat. Methods* 10: 57–59.
36. Amir, A., D. McDonald, J. A. Navas-Molina, E. Kopylova, J. T. Morton, Z. Zech Xu, E. P. Kightley, L. R. Thompson, E. R. Hyde, A. Gonzalez, and R. Knight. 2017. Deblur rapidly resolves single-nucleotide community sequence patterns. *mSystems* 2: e00191-16.
37. DeSantis, T. Z., P. Hugenholtz, N. Larsen, M. Rojas, E. L. Brodie, K. Keller, T. Huber, D. Dalevi, P. Hu, and G. L. Andersen. 2006. Greengenes, a chimera-checked 16S rRNA gene database and workbench compatible with ARB. *Appl. Environ. Microbiol.* 72: 5069–5072.
38. Mirarab, S., N. Nguyen, and T. Warnow. 2012. SEPP: SATé-enabled phylogenetic placement. *Pac. Symp. Biocomput.* DOI: 10.1142/9789814366496_0024.
39. Faith, D. P. 1992. Conservation evaluation and phylogenetic diversity. *Biol. Conserv.* 61: 1–10.
40. Lozupone, C., and R. Knight. 2005. UniFrac: a new phylogenetic method for comparing microbial communities. *Appl. Environ. Microbiol.* 71: 8228–8235.

41. Lozupone, C. A., M. Hamady, S. T. Kelley, and R. Knight. 2007. Quantitative and qualitative beta diversity measures lead to different insights into factors that structure microbial communities. *Appl. Environ. Microbiol.* 73: 1576–1585.
42. Chen, M. J., L. C. Chou, T. T. Hsieh, D. D. Lee, K. W. Liu, C. Y. Yu, Y. J. Oyang, H. K. Tsai, and C. Y. Chen. 2012. De novo motif discovery facilitates identification of interactions between transcription factors in *Saccharomyces cerevisiae*. *Bioinformatics* 28: 701–708.
43. Vázquez-Baeza, Y., M. Pirrung, A. Gonzalez, and R. Knight. 2013. EMPeror: a tool for visualizing high-throughput microbial community data. *Gigascience* 2: 16.
44. Vázquez-Baeza, Y., A. Gonzalez, L. Smarr, D. McDonald, J. T. Morton, J. A. Navas-Molina, and R. Knight. 2017. Bringing the dynamic microbiome to life with animations. *Cell Host Microbe* 21: 7–10.
45. Iwabuchi, K., C. Iwabuchi, S. Tone, D. Itoh, N. Tosa, I. Negishi, K. Ogasawara, T. Uede, and K. Onoé. 2001. Defective development of NK1.1+ T-cell antigen receptor alphabeta+ cells in zeta-associated protein 70 null mice with an accumulation of NK1.1+ CD3- NK-like cells in the thymus. *Blood* 97: 1765–1775.
46. Bhattacharjee, J., J. M. Kumar, S. Arindkar, B. Das, U. Pramod, R. C. Juyal, S. S. Majumdar, and P. Nagarajan. 2014. Role of immunodeficient animal models in the development of fructose induced NAFLD. *J. Nutr. Biochem.* 25: 219–226.
47. Bhattacharjee, J., M. Kirby, S. Softic, L. Miles, R. M. Salazar-Gonzalez, P. Shivakumar, and R. Kohli. 2017. Hepatic natural killer T-cell and CD8+ T-cell signatures in mice with nonalcoholic steatohepatitis. *Hepatol Commun* 1: 299–310.
48. Blériot, C., T. Dupuis, G. Jouvion, G. Eberl, O. Disson, and M. Lecuit. 2015. Liver-resident macrophage necroptosis orchestrates type 1 microbicidal inflammation and type-2-mediated tissue repair during bacterial infection. *Immunity* 42: 145–158.
49. Loomba, R., V. Seguritan, W. Li, T. Long, N. Klitgord, A. Bhatt, P. S. Dulai, C. Caussy, R. Bettencourt, S. K. Highlander, et al. 2017. Gut microbiome-based metagenomic signature for non-invasive detection of advanced fibrosis in human nonalcoholic fatty liver disease. *Cell Metab.* 25: 1054–1062.e5.
50. Caussy, C., C. Hsu, M. T. Lo, A. Liu, R. Bettencourt, V. H. Ajmera, S. Bassirian, J. Hooker, E. Sy, L. Richards, et al. 2018. Link between gut-microbiome derived metabolite and shared gene-effects with hepatic steatosis and fibrosis in NAFLD. *Hepatology* 68: 918–932.
51. Anderson, M. J. 2001. A new method for non-parametric multivariate analysis of variance. *Austral Ecol.* 26: 32–46.
52. Mandal, S., W. Van Treuren, R. A. White, M. Eggesbø, R. Knight, and S. D. Peddada. 2015. Analysis of composition of microbiomes: a novel method for studying microbial composition. *Microb. Ecol. Health Dis.* 26: 27663.
53. Selvanantham, T., Q. Lin, C. X. Guo, A. Surendra, S. Fieve, N. K. Escalante, D. S. Guttman, C. J. Streutker, S. J. Robertson, D. J. Philpott, and T. Mallevaey. 2016. NKT cell-deficient mice harbor an altered microbiota that fuels intestinal inflammation during chemically induced colitis. *J. Immunol.* 197: 4464–4472.
54. Ishioka, M., K. Miura, S. Minami, Y. Shimura, and H. Ohnishi. 2017. Altered gut microbiota composition and immune response in experimental steatohepatitis mouse models. *Dig. Dis. Sci.* 62: 396–406.
55. Zhu, L., S. S. Baker, C. Gill, W. Liu, R. Alkhouri, R. D. Baker, and S. R. Gill. 2013. Characterization of gut microbiomes in nonalcoholic steatohepatitis (NASH) patients: a connection between endogenous alcohol and NASH. *Hepatology* 57: 601–609.
56. Bandyopadhyay, K., I. Marrero, and V. Kumar. 2016. NKT cell subsets as key participants in liver physiology and pathology. *Cell. Mol. Immunol.* 13: 337–346.
57. Bedel, R., R. Berry, T. Mallevaey, J. L. Matsuda, J. Zhang, D. I. Godfrey, J. Rossjohn, J. W. Kappler, P. Marrack, and L. Gapin. 2014. Effective functional maturation of invariant natural killer T cells is constrained by negative selection and T-cell antigen receptor affinity. *Proc. Natl. Acad. Sci. USA* 111: E119–E128.
58. Koay, H. F., N. A. Gherardin, A. Enders, L. Loh, L. K. Mackay, C. F. Almeida, B. E. Russ, C. A. Nold-Petry, M. F. Nold, S. Bedoui, et al. 2016. A three-stage intrathymic development pathway for the mucosal-associated invariant T cell lineage. *Nat. Immunol.* 17: 1300–1311.
59. Hegde, P., E. Weiss, V. Paradis, J. Wan, M. Mabire, S. Sukriti, P. E. Rautou, M. Albuquerque, O. Picq, A. C. Gupta, et al. 2018. Mucosal-associated invariant T cells are a profibrogenic immune cell population in the liver. *Nat. Commun.* 9: 2146.
60. Satoh, M., Y. Andoh, C. S. Clingan, H. Ogura, S. Fujii, K. Eshima, T. Nakayama, M. Taniguchi, N. Hirata, N. Ishimori, et al. 2012. Type II NKT cells stimulate diet-induced obesity by mediating adipose tissue inflammation, steatohepatitis and insulin resistance. *PLoS One* 7: e30568.
61. Valenti, L., A. L. Fracanzani, and S. Fargion. 2009. The immunopathogenesis of alcoholic and nonalcoholic steatohepatitis: two triggers for one disease? *Semin. Immunopathol.* 31: 359–369.
62. Guebre-Xabier, M., S. Yang, H. Z. Lin, R. Schwenk, U. Krzych, and A. M. Diehl. 2000. Altered hepatic lymphocyte subpopulations in obesity-related murine fatty livers: potential mechanism for sensitization to liver damage. *Hepatology* 31: 633–640.
63. Locatelli, I., S. Sutti, M. Vacchiano, C. Bozzola, and E. Albano. 2013. NF-κB1 deficiency stimulates the progression of non-alcoholic steatohepatitis (NASH) in mice by promoting NKT-cell-mediated responses. *Clin. Sci. (Lond.)* 124: 279–287.
64. Yamagata, H., K. Ikejima, K. Takeda, T. Aoyama, K. Kon, K. Okumura, and S. Watanabe. 2013. Altered expression and function of hepatic natural killer T cells in obese and diabetic KK-A(y) mice. *Hepatol. Res.* 43: 276–288.
65. Vasseur, P., S. Dion, A. Filliol, V. Genet, C. Lucas-Clerc, G. Jean-Philippe, C. Silvain, J. C. Lecron, C. Piquet-Pellorce, and M. Samson. 2017. Endogenous IL-33 has no effect on the progression of fibrosis during experimental steatohepatitis. *Oncotarget* 8: 48563–48574.
66. Tang, T., Y. Sui, M. Lian, Z. Li, and J. Hua. 2013. Pro-inflammatory activated Kupffer cells by lipids induce hepatic NKT cells deficiency through activation-induced cell death. *PLoS One* 8: e81949.
67. Wilson, M. T., C. Johansson, D. Olivares-Villagómez, A. K. Singh, A. K. Stanic, C. R. Wang, S. Joyce, M. J. Wick, and L. Van Kaer. 2003. The response of natural killer T cells to glycolipid antigens is characterized by surface receptor down-modulation and expansion. *Proc. Natl. Acad. Sci. USA* 100: 10913–10918.
68. Harada, M., K. Seino, H. Wakao, S. Sakata, Y. Ishizuka, T. Ito, S. Kojo, T. Nakayama, and M. Taniguchi. 2004. Down-regulation of the invariant Valpha14 antigen receptor in NKT cells upon activation. *Int. Immunol.* 16: 241–247.
69. Emoto, M., T. Shimizu, H. Koike, I. Yoshizawa, R. Hurwitz, S. H. Kaufmann, and Y. Emoto. 2010. Dissociated expression of natural killer 1.1 and T-cell receptor by invariant natural killer T cells after interleukin-12 receptor and T-cell receptor signalling. *Immunology* 129: 62–74.
70. Rau, M., A. K. Schilling, J. Meertens, I. Hering, J. Weiss, C. Jurowich, T. Kudlich, H. M. Hermanns, H. Bantel, N. Beyersdorf, and A. Geier. 2016. Progression from nonalcoholic fatty liver to nonalcoholic steatohepatitis is marked by a higher frequency of Th17 cells in the liver and an increased Th17/resting regulatory T cell ratio in peripheral blood and in the liver. *J. Immunol.* 196: 97–105.
71. Harley, I. T., T. E. Stankiewicz, D. A. Giles, S. Softic, L. M. Flick, M. Cappelletti, R. Sheridan, S. A. Xanthakos, K. A. Steinbrecher, R. B. Sartor, et al. 2014. IL-17 signaling accelerates the progression of nonalcoholic fatty liver disease in mice. *Hepatology* 59: 1830–1839.
72. Syn, W. K., Y. H. Oo, T. A. Pereira, G. F. Karaca, Y. Jung, A. Omenetti, R. P. Witek, S. S. Choi, C. D. Guy, C. M. Fearing, et al. 2010. Accumulation of natural killer T cells in progressive nonalcoholic fatty liver disease. *Hepatology* 51: 1998–2007.
73. Lemmers, A., C. Moreno, T. Gustot, R. Maréchal, D. Degré, P. Demetter, P. de Nadai, A. Geerts, E. Quertinmont, V. Vercruysse, et al. 2009. The interleukin-17 pathway is involved in human alcoholic liver disease. *Hepatology* 49: 646–657.
74. Koyama, Y., and D. A. Brenner. 2017. Liver inflammation and fibrosis. *J. Clin. Invest.* 127: 55–64.
75. Meng, F., K. Wang, T. Aoyama, S. I. Grivennikov, Y. Paik, D. Scholten, M. Cong, K. Iwaisako, X. Liu, M. Zhang, et al. 2012. Interleukin-17 signaling in inflammatory, Kupffer cells, and hepatic stellate cells exacerbates liver fibrosis in mice. *Gastroenterology.* 143: 765–776.e3.
76. Tang, Y., Z. Bian, L. Zhao, Y. Liu, S. Liang, Q. Wang, X. Han, Y. Peng, X. Chen, L. Shen, et al. 2011. Interleukin-17 exacerbates hepatic steatosis and inflammation in non-alcoholic fatty liver disease. *Clin. Exp. Immunol.* 166: 281–290.
77. Gomes, A. L., A. Teijeiro, S. Burén, K. S. Tummala, M. Yilmaz, A. Waisman, J. P. Theurillat, C. Perna, and N. Djouder. 2016. Metabolic inflammation-associated IL-17A causes non-alcoholic steatohepatitis and hepatocellular carcinoma. *Cancer Cell* 30: 161–175.
78. Liu, Y., S. Munker, R. Müllenbach, and H. L. Weng. 2012. IL-13 signaling in liver fibrogenesis. *Front. Immunol.* 3: 116.
79. Li, H. Y., D. Ju, D. W. Zhang, H. Li, L. M. Kong, Y. Guo, C. Li, X. L. Wang, Z. N. Chen, and H. Bian. 2015. Activation of TGF-β1-CD147 positive feedback loop in hepatic stellate cells promotes liver fibrosis. *Sci. Rep.* 5: 16552.
80. Shimamura, T., T. Fujisawa, S. R. Husain, M. Kioi, A. Nakajima, and R. K. Puri. 2008. Novel role of IL-13 in fibrosis induced by nonalcoholic steatohepatitis and its amelioration by IL-13R-directed cytotoxin in a rat model. *J. Immunol.* 181: 4656–4665.
81. Ghazarian, M., X. S. Revelo, M. K. Nøhr, H. Luck, K. Zeng, H. Lei, S. Tsai, S. A. Schroer, Y. J. Park, M. H. Y. Chng, et al. 2017. Type I interferon responses drive intrahepatic T cells to promote metabolic syndrome. *Sci. Immunol.* 2: eaai7616.
82. Strodthoff, D., A. M. Lundberg, H. E. Agardh, D. F. Ketelhuth, G. Paulsson-Berne, P. Arner, G. K. Hansson, and N. Gerdes. 2013. Lack of invariant natural killer T cells affects lipid metabolism in adipose tissue of diet-induced obese mice. *Arterioscler. Thromb. Vasc. Biol.* 33: 1189–1196.
83. Ma, C., A. H. Kesarwala, T. Eggert, J. Medina-Echeverz, D. E. Kleiner, P. Jin, D. F. Stroncek, M. Terabe, V. Kapoor, M. ElGindi, et al. 2016. NAFLD causes selective CD4(+) T lymphocyte loss and promotes hepatocarcinogenesis. *Nature* 531: 253–257.
84. Kremer, M., E. Thomas, R. J. Milton, A. W. Perry, N. van Rooijen, M. D. Wheeler, S. Zacks, M. Fried, R. A. Rippe, and I. N. Hines. 2010. Kupffer cell and interleukin-12-dependent loss of natural killer T cells in hepatosteatosis. *Hepatology* 51: 130–141.
85. Stienstra, R., F. Saudale, C. Duval, S. Keshtkar, J. E. Groener, N. van Rooijen, B. Staels, S. Kersten, and M. Müller. 2010. Kupffer cells promote hepatic steatosis via interleukin-1beta-dependent suppression of peroxisome proliferator-activated receptor alpha activity. *Hepatology* 51: 511–522.
86. Seki, E., S. de Minicis, S. Inokuchi, K. Taura, K. Miyai, N. van Rooijen, R. F. Schwabe, and D. A. Brenner. 2009. CCR2 promotes hepatic fibrosis in mice. *Hepatology* 50: 185–197.
87. Miura, K., L. Yang, N. van Rooijen, H. Ohnishi, and E. Seki. 2012. Hepatic recruitment of macrophages promotes nonalcoholic steatohepatitis through CCR2. *Am. J. Physiol. Gastrointest. Liver Physiol.* 302: G1310–G1321.
88. Wei, Y., B. Zeng, J. Chen, G. Cui, C. Lu, W. Wu, J. Yang, H. Wei, R. Xue, L. Bai, et al. 2016. Enterogenous bacterial glycolipids are required for the generation of natural killer T cells mediated liver injury. *Sci. Rep.* 6: 36365.

89. Hritz, I., P. Mandrekar, A. Velayudham, D. Catalano, A. Dolganiuc, K. Kodys, E. Kurt-Jones, and G. Szabo. 2008. The critical role of toll-like receptor (TLR) 4 in alcoholic liver disease is independent of the common TLR adapter MyD88. *Hepatology* 48: 1224–1231.
90. Adler, M., S. Taylor, K. Okebugwu, H. Yee, C. Fielding, G. Fielding, and M. Poles. 2011. Intrahepatic natural killer T cell populations are increased in human hepatic steatosis. *World J. Gastroenterol.* 17: 1725–1731.
91. Tajiri, K., Y. Shimizu, K. Tsuneyama, and T. Sugiyama. 2009. Role of liver-infiltrating CD3+CD56+ natural killer T cells in the pathogenesis of nonalcoholic fatty liver disease. *Eur. J. Gastroenterol. Hepatol.* 21: 673–680.
92. Xu, C. F., C. H. Yu, Y. M. Li, L. Xu, J. Du, and Z. Shen. 2007. Association of the frequency of peripheral natural killer T cells with nonalcoholic fatty liver disease. *World J. Gastroenterol.* 13: 4504–4508.
93. Van Der Vliet, H. J., N. Nishi, Y. Koezuka, M. A. Peyrat, B. M. Von Blomberg, A. J. Van Den Eertwegh, H. M. Pinedo, G. Giaccone, and R. J. Scheper. 1999. Effects of alpha-galactosylceramide (KRN7000), interleukin-12 and interleukin-7 on phenotype and cytokine profile of human Valpha24+ Vbeta11+ T cells. *Immunology* 98: 557–563.
94. Gutowska-Owsiak, D., M. A. Birchall, R. J. Moots, S. E. Christmas, and L. Pazmany. 2014. Proliferatory defect of invariant population and accumulation of non-invariant CD1d-restricted natural killer T cells in the joints of RA patients. *Mod. Rheumatol.* 24: 434–442.
95. Swiecki, M., S. Gilfillan, W. Vermi, Y. Wang, and M. Colonna. 2010. Plasmacytoid dendritic cell ablation impacts early interferon responses and antiviral NK and CD8(+) T cell accrual. *Immunity* 33: 955–966.
96. Mandl, M., M. Drechsler, Y. Jansen, C. Neideck, H. Noels, A. Faussner, O. Soehnlein, C. Weber, and Y. Döring. 2015. Evaluation of the BDCA2-DTR transgenic mouse model in chronic and acute inflammation. *PLoS One* 10: e0134176.
97. Arora, P., A. Baena, K. O. Yu, N. K. Saini, S. S. Kharkwal, M. F. Goldberg, S. Kunnath-Velayudhan, L. J. Carreño, M. M. Venkataswamy, J. Kim, et al. 2014. A single subset of dendritic cells controls the cytokine bias of natural killer T cell responses to diverse glycolipid antigens. *Immunity* 40: 105–116.
98. Marschner, A., S. Rothenfusser, V. Hornung, D. Prell, A. Krug, M. Kerkmann, D. Wellisch, H. Poeck, A. Greinacher, T. Giese, et al. 2005. CpG ODN enhance antigen-specific NKT cell activation via plasmacytoid dendritic cells. *Eur. J. Immunol.* 35: 2347–2357.
99. Pirola, C. J., T. F. Gianotti, A. L. Burgueño, M. Rey-Funes, C. F. Loidl, P. Mallardi, J. S. Martino, G. O. Castaño, and S. Sookoian. 2013. Epigenetic modification of liver mitochondrial DNA is associated with histological severity of nonalcoholic fatty liver disease. *Gut* 62: 1356–1363.
100. Koliaki, C., J. Szendroedi, K. Kaul, T. Jelenik, P. Nowotny, F. Jankowiak, C. Herder, M. Carstensen, M. Krausch, W. T. Knoefel, et al. 2015. Adaptation of hepatic mitochondrial function in humans with non-alcoholic fatty liver is lost in steatohepatitis. *Cell Metab.* 21: 739–746.
101. Garcia-Martinez, I., N. Santoro, Y. Chen, R. Hoque, X. Ouyang, S. Caprio, M. J. Shlomchik, R. L. Coffman, A. Candia, and W. Z. Mehal. 2016. Hepatocyte mitochondrial DNA drives nonalcoholic steatohepatitis by activation of TLR9. *J. Clin. Invest.* 126: 859–864.
102. Handa, P., A. Vemulakonda, K. V. Kowdley, M. Uribe, and N. Méndez-Sánchez. 2016. Mitochondrial DNA from hepatocytes as a ligand for TLR9: drivers of nonalcoholic steatohepatitis? *World J. Gastroenterol.* 22: 6965–6971.
103. Diana, J., Y. Simoni, L. Furio, L. Beaudoin, B. Agerberth, F. Barrat, and A. Lehuen. 2013. Crosstalk between neutrophils, B-1a cells and plasmacytoid dendritic cells initiates autoimmune diabetes. *Nat. Med.* 19: 65–73.
104. Everts, B., R. Tussiwand, L. Dreesen, K. C. Fairfax, S. C. Huang, A. M. Smith, C. M. O'Neill, W. Y. Lam, B. T. Edelson, J. F. Urban, Jr, et al. 2016. Migratory CD103+ dendritic cells suppress helminth-driven type 2 immunity through constitutive expression of IL-12. *J. Exp. Med.* 213: 35–51.
105. Mowat, A. M., and W. W. Agace. 2014. Regional specialization within the intestinal immune system. *Nat. Rev. Immunol.* 14: 667–685.
106. Lukacs-Kornek, V., and D. Schuppan. 2013. Dendritic cells in liver injury and fibrosis: shortcomings and promises. *J. Hepatol.* 59: 1124–1126.
107. Osmond, T. L., K. J. Farrand, G. F. Painter, C. Ruedl, T. R. Petersen, and I. F. Hermans. 2015. Activated NKT cells can condition different splenic dendritic cell subsets to respond more effectively to TLR engagement and enhance cross-priming. *J. Immunol.* 195: 821–831.
108. Shimizu, K., M. Asakura, J. Shinga, Y. Sato, S. Kitahara, K. Hoshino, T. Kaisho, S. P. Schoenberger, T. Ezaki, and S. Fujii. 2013. Invariant NKT cells induce plasmacytoid dendritic cell (DC) cross-talk with conventional DCs for efficient memory CD8+ T cell induction. *J. Immunol.* 190: 5609–5619.
109. Kelly, A., R. Fahey, J. M. Fletcher, C. Keogh, A. G. Carroll, R. Siddachari, J. Geoghegan, J. E. Hegarty, E. J. Ryan, and C. O'Farrelly. 2014. CD141^{+} myeloid dendritic cells are enriched in healthy human liver. *J. Hepatol.* 60: 135–142.
110. Romano, K. A., E. I. Vivas, D. Amador-Noguez, and F. E. Rey. 2015. Intestinal microbiota composition modulates choline bioavailability from diet and accumulation of the proatherogenic metabolite trimethylamine-N-oxide. *MBio* 6: e02481.
111. Morton, J. T., J. Sanders, R. A. Quinn, D. McDonald, A. Gonzalez, Y. Vázquez-Baeza, J. A. Navas-Molina, S. J. Song, J. L. Metcalf, E. R. Hyde, et al. 2017. Balance trees reveal microbial niche differentiation. *mSystems* 2: e00162-16.